Accepted Manuscript
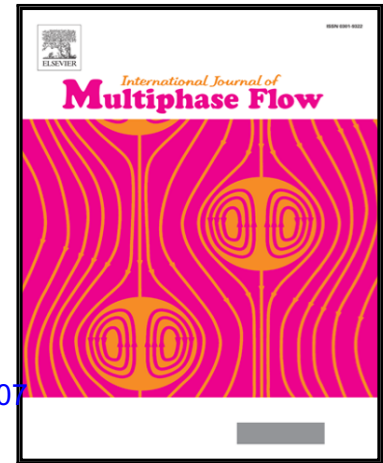
The Hydrodynamics of Two-Phase Flows in the Injection Part of a Conventional Ejector

D. Mifsud, Y. Cao, P.G. Verdin, L. Lao

The Hydrodynamics of Two-Phase Flows in the Injection Part of a Conventional Ejector

D. Mifsud[a,*], Y. Cao[b], P. G. Verdin[a], L. Lao[a]

[a]*Geo-Energy Engineering Centre, School of Water, Energy and Environment Cranfield University, Cranfield, MK43 0AL, UK*
[b]*College of Chemical and Biological Engineering, Zhejiang University,Hangzhou, 310027, P. R. China*

Abstract

The characteristics of two-phase flow through a 'conventional' convergent-nozzle in an entrainment chamber of an ejector apparatus are described in this paper. A unique data set comprising 350 data points was generated in an air-water horizontal test-rig. Two sets of flow conditions were established, the first one including high liquid - low gas fluids with void fractions less than 0.55, and the second one involving high gas - low liquid fluids with void fractions greater than 0.75. All considered flow-rates lied within the sub-critical flow region. Two-phase flow pressure drop multiplier based empirical correlations were developed to estimate the total mass flow-rates. In the high liquid region, Morris (1985) correlation was modified, resulting in less than 10 % error. In the high gas region, two new correlations were proposed, showing less than 10 % and 15 % of errors, respectively. The established empirical correlations were related to other available multipliers for different geometric configurations including a Venturi, an orifice plate, a gate valve, and a globe valve and were compared to 20 other void fraction correlations. The Chisholm (1983) and Huq and Loth (1992) correlations showed the highest similarities to the ones proposed for the high liquid and high gas regions, respectively.

Key words:
Mach number, converging-nozzle, jet pump, compressibility-factor, pressure-drop multiplier, void fraction.

1. Introduction

Most of the industrial equipment designed to handle single or multiphase fluids have geometric features that attribute unique flow dynamic characteristics. Industrial process facilities involve networks of pipelines characterised by several devices and pipe fittings of various geometrical configurations. Typical components include elbows, valves, annular pipe sections, pipe reducers such as nozzles and orifice plates, expanders such as diffusers, and other complex pipe sections such as helical and spiral pipes. The referred fittings and devices are primarily installed for specific purposes, such as to give flexibility to the system, to condition processing fluids or to enact control.

Several authors have in the past understood that studying the fluid behaviour across a specific geometric configuration was an opportunity to develop simple methods in aid to: (1) estimate the total mass flow-rates, (2) facilitate other relevant process fluid dynamics, such as phase separation along blind corners or mixing along specially designed test pieces. Some of the most significant literature includes the work of Fairhurst (1983) who studied the pressure loss for both single and two-phase fluids across globe valves, gate valves and orifice plates. Smoglie and Reimann (1986) studied the two-phase flow discharge through branches of various orientations along a horizontal main conduit, specifically including T-junctions. Silva et al. (1991) investigated a Venturi tube to estimate the total mass flow-rates of multiphase fluids. McNeil (2000) developed a generic model applicable for all pipe fittings of the contraction-expansion type, able to estimate the total mass flow-rates up to choking conditions. Azzi et al. (2000) studied the fluid dynamics of two-phase flow pressure loss in 180° bends. Fossa and Guglielmini (2002) studied pressure-drop and void fraction across thin and thick orifices. Alimonti et al. (2010) investigated the characteristics of two-phase flows through a "Willis-type" multiple orifice valve (MOV), while Azzi and Friedel (2005), Chen et al. (2006) and Kim et al. (2010) evaluated the use of 90° elbows as primary elements to estimate the total mass flow-rates. Additionally, Xing et al. (2013) performed a study comprising wavy pipe sections to mitigate slug flow regimes. Gourma and Verdin (2016) investigated the influence of helical pipes on slugs while Athulya and Miji Cherian (2016) numerically studied multiphase flows in a T-junction.

----

*Corresponding Author.

E-mail: d.mifsud@cranfield.ac.uk (D. Mifsud)

The focus of this work entails the hydrodynamic characteristic of both single and two-phase flows through a conventional-design convergent nozzle fixed within a vacuum chamber of an educator/jet pump device. This device, as illustrated in figure 1, is used to convert the potential energy of a high-pressure fluid to dynamic energy, thus creating a high-speed jet propagating from the nozzle throat towards the throat-inlet.
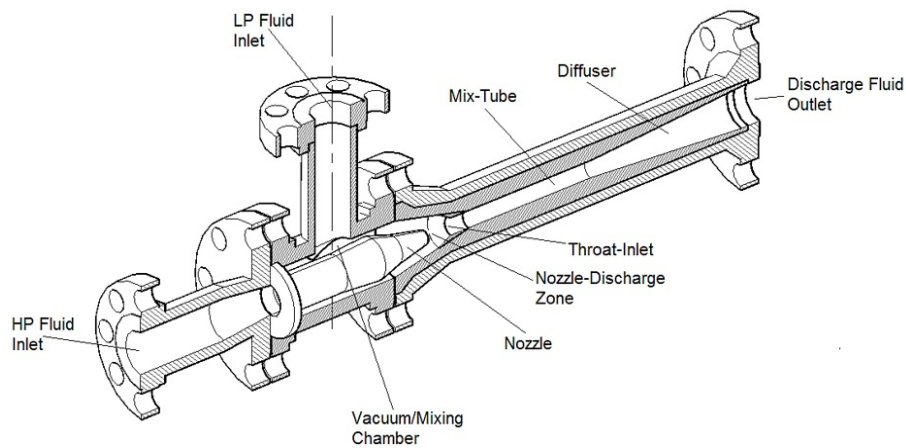

Figure 1: Schematic illustration of a typical conventionally-designed eductor/jet pump.In figure, LP and HP denotes Low Pressure and High Pressure respectively.

The high-speed jet creates a low-pressure zone within the vacuum/mixing chamber which will, as a result, entrain a low-pressure fluid into the mixing chamber. Both fluids will then mix partially along the throat-inlet, and will be presumed to mix fully by the end of the mix-tube section. The mixture will then flow through the diffuser part to undergo a recovery of static pressure. Under normal/effective performance operations, the discharge pressure of the mixture flow comprises a pressure lower than the motive fluid but higher than the production fluid, thus, creating a boost. The educator/jet-pump technology is a well-known and available technology for several processes involving the pumping and mixing of fluids, while it is still gaining popularity within the oil and gas industry. The development of this technology significantly increased in the last decade as oil and gas producers have been seeking to invest in cheap and effective Improved Oil Recovery (IOR) and Enhanced Oil Recovery (EOR) solutions. Mali et al. (2013) proved that this technology was the cheapest (in terms of both capital and operations expenditure) among all other artificial lift solutions, and Sarshar (2012) stated that a new jet pump installation in the indefatigable oil and gas sector gave a pay-back period of less than 10 days. In parallel to the

development of this technology, the oil and gas industry is still looking for the development of cost-effective flow monitoring devices, incurring simplistic forms of metering methods, which are practicable and economic feasible for installation at multiple wellheads (Falcone et al., 2001). One method is to enhance control by monitoring the production flow of each well, rather than monitoring one production flow. Currently, most production facilities use a single wellhead choke valve to monitor and control the total production flow rate. A patent from Beg and Sarshar (2015) describes a system which can be used for production boosting and flow-rate measurement in a pipeline, for applications in the oil and gas industry. This includes a configuration involving the use of a jet pump device to measure flow-rates when operated under single-phase (gas or fluid) flows. The fluid characteristics inside such device are however not fully understood yet. It is therefore of utmost importance to study such behaviour under multi-phase flow conditions.

Gaining knowledge of the hydrodynamic fluid behaviour in a jet pump can help developing an apparatus primarily installed for enhancing and boosting the relative low-pressure fluid sources, which could also act as a flow monitoring device. This could lead to a novel form to estimate the total mass flow-rates of either the motive only, or both the motive and production fluids. The overall performance of a typical device is the combined result of the entrainment of low-pressure fluid and boost. This performance is therefore the resultant of the hydrodynamic fluid behaviour, mainly of the energy and momentum transfer of the driving single-phase (or multiphase) jet. The behaviour of single-phase (gas or liquid) jets is well understood but the behaviour of multiphase-produced jets from convergent nozzles is not easily predictable, and vary drastically in regions of high gas-low liquid and high liquid-low gas two-phase flow combinations. The two-phase fluid behaviour in a jet pump will be investigated. Two-phase flows are characterised by: (1) larger pressure drops due to compressibility effects during contraction and expansion of gas, (2) significant variances in mixture density with the increase of flow quality, (3) phase slip and (4) significant variances in coefficient of discharge comprising all irreversible energy losses. The work presented in this paper aims at gaining knowledge of the two-phase flow hydrodynamic behaviour, specifically along the injection part of a conventional eductor device. To achieve such objectives, the following tasks have been performed: (1) review of existing models used for calculating multiphase flows in general flow conditions, (2) develop a unique dataset comprising the conventional design convergent nozzle, (3) determine the behaviour of single and two-phase air-water discharge loss coefficients, (4) determine empirical two-phase

air-water frictional pressure drop multipliers for both high liquid-low gas of void fraction $0 < \alpha \leq 0.55$ (having flow combinations involving liquid-water and gas-air flow-rates of: 0.25 - 2.0 kg/s and 5 - 100 Slpm respectively), and high gas-low liquid flow regions of $0.75 \leq \alpha < 1$ (having flow combinations involving liquid-water and gas-air flow-rates of: 0 - 500 Slpm and 5-300 Sm^3/hr respectively), (5) appraise and improve the developed two-phase models, and (6) assess and compare the developed two-phase multipliers against other standard geometries encountered in the oil and gas sector.

2. Theoretical Background

Several models have been developed to correlate the pressure loss and the two-phase flow-rates for sub-critical and critical conditions. 'Critical conditions' refer to the point where a maximum single or multiphase fluid flow-rate is attained at a given upstream pressure. Four categories are available to estimate the total mass flow at sub-critical and/or critical choking conditions. The first category comprises critical flow models based on empirical correlations from the Gilbert (1954) critical choke equation. In-contrast to all other models, this category estimates the critical total mass flow-rates via the upstream (well-head) pressure only. Thereby, the empirical parameters are not dependent on the pressure loss across the choke valves. Such methodology differs from the scope of this work. The second category comprises theoretical derivations based on fundamental principles and general equations. This category includes choke flow model correlations used to estimate total mass flow-rates at sub-critical and critical flow conditions. Such models are derived from theoretical equations based on the conservation of mass, energy and momentum. Authors have presented different approaches to account for compressibility effects. Tangren et al. (1949) worked on a homogeneous flow model, totally neglecting the flashing of gas from the liquid phase downstream of the choke. Grolmes and Fauske (1970) and Henry and Fauske (1971) presented two homogeneous flow models considering thermal equilibrium. Within the past 30 years, the five most popular models for estimating the total mass flow rate of multiphase flows were established by (1) Sachdeva et al. (1986) who developed a very simplistic model involving the use of the homogeneous density equation thus no slip, (2) Perkins (1993) who developed a model based on the gas-phase energy equation rather than the multiphase momentum equation and proved valid for the estimation of both critical and sub-critical flow-rates, (3) Selmer-Olsen and Lemonnier (1995) who developed the so called 'Hydro Model' comprising two sub models

referred as the long and short mechanistic models which use the momentum density equation and consider slip, (4) Alsafran and Kelkar (2009) who proposed a refined model of the Sachdeva et al. (1986) approach in which a pressure recovery term was introduced and slip between phases was considered, and (5) Asheim's model as given in the work of Haug (2012) which involves the integration of the Bernoulli relationship, expressing the homogeneous mixture via the ideal gas law, but totally neglecting phase slippage and downstream pressure recovery. The third category involves the frictional two-phase pressure drop multiplier Φ_{LO}^2. This methodology is highly relevant to this work. This method is based on the classical single-phase approach, where a single-phase incompressible relationship is primarily used to generate a correlation for the two-phase pressure drop multiplier. Thereby the two-phase pressure drop Δp_{mix} is related to the actual pressure difference for the liquid flow alone, ΔP_{LO}, via the two-phase pressure drop multiplier Φ_{LO}^2. The referenced models consider the two-phase frictional pressure drop multiplier as a multiplier which accounts for all loss components attributed to two-phase flows, including mainly compressibility effects, molecular interaction between phases, acoustic losses, resistance losses due to parts acting as bluff bodies, and frictional losses such as surface roughness. Several models have been developed to predict the frictional pressure drop multiplier under two-phase operating conditions. Six of the most common and well applicable models are described below:

1. The homogeneous equilibrium model [HEM] (Green and Perry, 1973).

   The HEM neglects slip between the two-phase (gas-liquid) flows. The HEM correlation is expressed as:

$$\Phi_{LO}^2 = 1 + x\left[\frac{\rho_L}{\rho_G} - 1\right] \tag{1}$$

   where x is the flow quality, while ρ_L and ρ_G denote the liquid and gas densities respectively.

2. The Simpson et al. (1983) model

   This model expresses the two-phase frictional pressure drop in terms of slip S_S and vapour quality x.

$$\Phi_{LO}^2 = x\left(x\frac{\rho_L}{\rho_G} + S_S(1-x)\right)\left(x\frac{1-x}{S_s}\right) \tag{2}$$

   where the slip S_S, as proposed by Simpson et al. (1983) is given by:

$$S_S = \left[\frac{\rho_L}{\rho_G} \right]^y \tag{3}$$

The exponent *y* varies from 0 in case of no slip for a homogeneous flow, and reaches a maximum slip value of 0.5. Based on experimental trials, Simpson et al. (1983) proposed an averaged value of 1/6. This slip expression neglects the use of vapour quality *x*, but considers only the ratio of phase densities.

3. The Lockhart and Martinelli (1949) model (Taitel and Dukler, 1976).

This method considers the two-phase (air-gas) flow as totally separated flows. Hence a relationship is expressed for the gas phase and another one for the liquid phase. The two-phase frictional pressure drop multiplier is given by:

$$\Phi^2_{LO} = 1 + \left(\frac{CL}{X_P} \right) + \left(\frac{1}{X_P^2} \right) \tag{4}$$

where *CL* is a function of the flow regime, and X_P is the Lockhart Martinelli parameter expressed as:

$$X_P^2 = \frac{(dp/dz)_L}{(dp/dz)_G} \tag{5}$$

with

$$(dp/dz)_L = f_L * \left(\frac{(2G^2(1-x^2))}{D\rho_L} \right) \tag{6}$$

and

$$(dp/dz)_G = f_G * \left(\frac{(2G^2(x^2))}{D\rho_G} \right) \tag{7}$$

where *D* is the throat diameter, f_L and f_G are the phase friction factors of liquid and gas respectively, *x* is the flow quality, and *G* is the total mass flux.

4. The Chisholm (1983) model.

Chisholm's correlation accounts for slip and is expressed by:

$$\Phi^2_{LO} = 1 + \left(\frac{\rho_L}{\rho_G} - 1 \right) \left[B*x(1-x) + x^2 \right] \tag{8}$$

This correlation takes into account two types of chokes, the short choke and the long choke,

the latter having a contraction length of more than half its diameter. This is performed using a parameter *B*, which is written as:

$$B = \frac{\left(\frac{1}{S_{ch}}\right)\left(\frac{\rho_L}{\rho_G}\right)+S_{ch}-2}{\left(\frac{\rho_L}{\rho_G}-1\right)}$$ (9)

given

$$S_{ch} = \begin{cases} \left(\frac{\rho_L}{\rho_H}\right)^{1/2} \\ \left(\frac{\rho_L}{\rho_G}\right)^{1/4} \end{cases} = \sqrt{1 + x\left(\frac{\rho_L}{\rho_G} - 1\right)}$$ (10)

where S_{ch} refers to the Chisholm slip ratio and ρ_H refers to the homogeneous (air-water) two-phase density.

5. The Alimonti et al. (2010) model.

   This model was proposed for the hydrodynamic characteristics of two-phase flow through an air-water multiple orifice valve (MOV), a replica of 'Willis'' choke valve. The illustrated two-phase multiplier expression follows the same method as the one applicable for the two-phase multiplier used to predict pressure loss in pipes.

$$\Phi_{LO}^2 = \frac{C}{(1-\xi)^n}$$ (11)

   where ξ refers to the void fraction and the parameters *C* and *n* are established through experimental calibration.

6. The Morris (1985) model.

   The correlation developed by Morris for the two-phase pressure drop multiplier accounts for the slippage of the (gas-liquid) two-phase flow. This correlation makes use of the Chisholm slip ratio S_{ch}, given in equation (10), and is dependent on the vapour quality *x* and density ratio $\frac{\rho_L}{\rho_G}$. Morris two-phase multiplier expression follows:

$$\Phi_{LO}^2 = \left(x\frac{\rho_L}{\rho_G} + S_{ch}(1-x)\right)\left[x + \frac{(1-x)}{S_{ch}}\left(1 + \frac{(S_{ch}-1)^2}{\left(\frac{\rho_L}{\rho_G}\right)^{1/2}}\right)\right]$$ (12)

Finally, the fourth category available to estimate the total mass flow at sub-critical or/and critical choking conditions includes models which estimate the total mass flow-rates via relationships that comprise both fundamental theory and correction factors obtained from empirical correlations. Such models were developed for the estimation of two-phase flows through safety

relief valves (SRV). The behaviour of complex phenomena occurring in constriction of safety relief valves is identical to those present in other constrictions. These models are slightly different from the two-phase pressure drop multiplier methodology described in this work, since they include two important parameters which are estimated separately: (1) the two-phase discharge coefficient, and (2) the two-phase compressibility factor. The two-phase compressibility factor is either included solely for the gas phase, or for both gas and vapour resulting from flashing liquid. The flashing refers to the sudden evaporation (change-of phase) of liquid when it experiences a sudden pressure drop. This phenomenon occurs under massive thermodynamic and mechanical non-equilibrium by variance of both temperature and phases velocities.

Several studies have also been performed to develop relationships for the two-phase discharge coefficient $C_{D_{TP}}$. Lenzing et al. (1998) presented a formulation which reflects the homogeneous flow of phases and considered the void fraction in the throat of a nozzle α_2, thereby including a discharge coefficient which is a function of the two-phase flow conditions. However, Leung (2004) formulation states that the two-phase discharge coefficient is a function of the liquid discharge coefficient and the ω-parameter, this parameter being introduced by the same author in 1994. Darby (2004) showed that under critical conditions the two-phase discharge coefficient is equal to the gas discharge coefficient, while when the two-phase flow is within the sub-critical conditions, the liquid discharge coefficient is used.

Among the above formulations, the Lenzing et al. (1998) two-phase discharge coefficient remains widely applicable. Lenzing's expression is written as:

$$C_{D_{TP}} = (\alpha_2) C_{D_g} + (1 - \alpha_2) C_{D_l} \tag{13}$$

where C_{D_l} and C_{D_g} denote the discharge coefficients of pure liquid and pure gas respectively. It is noted that in the case of gas, a constant value $C_{D_g} = 0.975$ is recommended by America Petroleum Institute (API), while for liquids, the coefficient tends to always be less than that of the gas under the same inlet conditions. The liquid coefficient is commonly estimated from experiments, with typical values ranging between 0.85-0.93. This variation of discharge coefficients therefore implies that the contraction of the flow must always be density dependant. To account for this, Darby and Molavi (1997) included a viscosity correction factor K_{vis} in equation (13).

$$C_{D_{TP}} = (\alpha_2) C_{D_g} + (1 - \alpha_2) C_{D_l} K_{vis} \tag{14}$$

Both authors found that $K_{vis} \rightarrow 1$ for viscosities < 100 mPa*s.

For the two-phase pressure drop multiplier expressions described here, the Homogeneous Non-Equilibrium Model (HNE-DS) developed by Diener and Schmidt (2004) was considered. This model is an improved model of the original (HNE) model derived by Henry, Fauske, and McComas (1970). The HNE-DS model entails the combination of measurement, thereby including: (1) a two-phase discharge coefficient $C_{D_{TP}}$ (based on the Lenzing et al. (1998) formulation), (2) a compressibility factor w (originally based on the Leung (2004) formulation), which includes both expansion and contraction effects caused by the two-phase flow, and (3) a flashing two-phase flow determined by the boiling delay factor N (extended version of Leung (2004) formulation), and a slip factor S.

Hence the total mass flow-rate $\dot{M}_{HNE-DS}$ is given by an equation comprising two parts: (1) an empirical portion which contains expressions derived from experimental based correlations including a two-phase discharge coefficient and a slip factor S, and (2) a fundamental portion which includes compressibility effects.

This can be written as:

$$\dot{M}_{HNE-DS} = \gamma_{corr} . A_n . \dot{m}_{HNE-DS} \tag{15}$$

with

$$\gamma_{corr} = C_{D_{TP}} . S \tag{16}$$

where A_n denotes the cross-sectional area at the nozzle throat, $\dot{m}_{HNE-DS}$ is the mass flux for isentropic frictionless flow, and is expressed by:

$$\dot{m}_{HNE-DS} = \Gamma \sqrt{\frac{2P_1}{v_0}} \tag{17}$$

where P_1 and v_0 are the pressure and specific volume of the mixture at absolute conditions (upstream throat) respectively. Γ is an outflow function expressed as:

$$\Gamma = \frac{\sqrt{w \ln\left(\frac{1}{Y}\right) - (w-1)(1-Y)}}{\left[w\left(\frac{1}{Y} - 1\right) + 1\right]} \tag{18}$$

The pressure ratio Y is the pressure at the nozzle throat P_2 divided by the absolute pressure

P_1, and w denotes the compressibility factor for non-equilibrium conditions given by equation (19). Note that this non-equilibrium relationship is valid for short-throat constrictions such as nozzles and thin orifices, i.e. for geometries showing a relative small area ratio. In these cases, a rapid pressure reduction occurs over a very short length of conduit, thus not providing sufficient time to reach equilibrium.

$$w = \frac{\alpha_1 v_{g1}}{v_1} + cp_{l,1}T_1P_1\left(\frac{v_{g,1}-v_{l,1}}{\Delta h_{v,1}^2}\right)^2. \; N \tag{19}$$

where α_1, $v_{g,1}$, $v_{l,1}$, $cp_{l,1}$, T_1 and $\Delta h_{v,1}$ denote the void fraction, specific volume of gas and liquid, specific heat capacity of liquid, temperature and latent heat of vaporisation at absolute conditions respectively, and N stands for the boiling density factor.

In the case of a flashing two-phase flow, the magnitude of the w parameter is characterised by the boiling density factor N, which varies between 0 (for thermodynamic equilibrium) and 1 (for the total boiling delay with no flashing of liquid). In this study, a value $N = 0$ is considered since the pressure at the throat of the nozzle (thus the pressure reduction), never reaches the critical vapour pressures (recorded at corresponding temperatures). This removes the second term of equation (19) and only the first term remains.

Additionally, to validate the applicability of the proposed correlations (in terms of void fraction), a comparison was performed against 20 other void fraction models.

The void fraction models and correlations considered in this study include three out of the four model-types categorised by Woldesemayat and Ghajar (2007).

The ones included in this study comprise homogeneous models, slip flow models and other empirical correlations models. All equations are detailed in table 1 and table 2. Note that the drift flux models were not considered in this study since all experiments were carried out in a horizontal test section having small diameter pipes of not more than 2 inches. In the case of slip void fraction models (model numbers 1-15 in table 1 and table 2), the void fraction α was estimated via the generic relationship:

$$\alpha = \left(1 + \left(\frac{1-x}{x}\right)\left(\frac{\rho_g}{\rho_l}\right)S\right)^{-1} \tag{20}$$

The slip ratio S is provided by another correlation, originally empirically derived correlation based on experimental data for gas-liquid mixtures at atmospheric pressure. This correlation,

proposed by Martinelli (1948) was expressed in terms of a dimensionless parameter, which is a function of mass dryness fraction, density and viscosity. For such equation, Smith (1969) stated that this correlation represented the very first real attempt at providing the designer with a generalised expression for predicting void fraction.

This equation was slightly modified by Baroczy (1963), Butterworth (1975), and Grolmes and Leung (1985) who established the following equation:

$$S = a_0 \left(\frac{1-x}{x} \right)^{(a_1-1)} \left(\frac{\rho_l}{\rho_g} \right)^{(a_2+1)} \left(\frac{\mu_l}{\mu_g} \right)^{(a_3)} \qquad (21)$$

where constants a_0, a_1, a_2, and a_3 are numerical constants given in table 1, $\left(\frac{\rho_l}{\rho_g} \right)$, and $\left(\frac{\mu_l}{\mu_g} \right)$ are the density ratio and dynamic viscosity ratios of liquid and gas.

Table 2 includes the other eight referenced void fraction models: (a) the rest of slip-based models (1, 14-15), (b) the homogeneous models (16-19), and (c) an empirical based model (20). Note that model numbers 1, 14 and 15 include the slip correlation, thus values of S are substituted in equation (20), while the other models involve an expression which denotes the void fraction α directly.

The applicability of each model is based on the comprehensive void fraction models comparison study performed by Mathure (2010), this is summarised in the last column of tables 1 and 2. Three performance categories can be defined: (1) moderate (percentage of data < 50 % of total and predicted within +/- 10 % error margin), (2) satisfactory (percentage of data > 50 but < 90 % of total and predicted within +/- 10 % error margin) and (3) exceptionally good (percentage of data > 95 % of total and predicted within +/- 10 % error margin).

Table 1: Values of a_0 a_1 a_2 and a_3 for use in Grolmes and Leung (1985) equation

No.	Model	a_0	a_1	a_2	a_3	Type	Details
3	Hom*	1	1	-1	0	Hom*	Multiple orientation including horizontal air-water
							Perform moderately for $\alpha \leq 0.50$ and $\alpha \geq 0.75$
2	Simpson et al. (1983)	1	1	-5/6	0	Slip	Horizontal pipes with large diameter (up to 127 mm) at qualities x < 0:005
4	Fauske (1961)	1	1	-1/2	0	Slip	Unknown orientation
							Perform moderately for $\alpha \geq 0.75$
5	Moody (1965)	1	1	-2/3	0	Slip	Horizontal - annular flow
							Local qualities 0.01 to 1.00
6	Baroczy (1966)	1	0.74	-0.65	0.13	Slip	Horizontal straight-tube
							Perform satisfactory for $\alpha \geq 0.75$
7	Lockart and Martinelli (1949)	0.28	0.64	-0.36	0.07	Slip	Horizontal air-water
							Perform moderately for $\alpha \leq 0.25$ $0.50 \leq \alpha \leq 0.75$ and exceptional good for $\alpha \geq 0.75$
8	Thom (1964)	1	1	-0.89	0.18	Slip	Vertical air-water
							Generically applied, but not predictable for low values of mass dryness fraction
							Perform satisfactory for $\alpha \geq 0.75$
9	Zivi (1964)	1	1	-0.67	0	Slip	Unknown orientation
							Perform satisfactory for $\alpha \geq 0.75$
10	Turner and Wallis (1965)	1	0.72	-0.4	0.08	Slip	Unknown orientation
							Perform moderate for $\alpha \geq 0.75$
11	Hamersma and Hart (1987)	0.26	0.67	-0.33	0	Slip	Horizontal air-water
							Perform moderately for $\alpha \geq 0.75$
12	Spedding and Chen (1984)	2.22	0.65	-0.65	0	Slip	Horizontal air-water
							Perform moderate for $\alpha \leq 0.25$ and satisfactory for $\alpha \geq 0.75$
13	Chen (1986)	0.18	0.6	-0.33	0.07	Slip	Extended formula of Spedding and Chen (1984)
							Perform moderate for $0.25 \leq \alpha \leq 0.50$ and satisfactory for $\alpha \geq 0.75$

Hom* - Homogeneous void fraction model types.

Table 2: Other referenced void fraction model-types

No.	Model	Relationship	Type	Details
		Other slip model-types		
1	Chisholm (1983)	$S = \left(1 - x\left(1 - \frac{\rho_l}{\rho_g}\right)\right)^{1/2}$	Slip	Horizontal gas/oil/water Performed satisfactorily for both $\alpha \leq 0.25$ and $\alpha \geq 0.75$
14	Schüller et al. (2003)	$S = \left(1 + x\left(\frac{\rho_l}{\rho_g} - 1\right)\right)^{1/2}\left(1 + \varepsilon e^{-\beta x}\right)$	Slip	Horizontal gas/oil/water Improved model for low gas qualities
15	Smith (1969)	$S = 0.4 + 0.6\left[\frac{\left(\frac{\rho_l}{\rho_g} + 0.4\left(\frac{1-x}{x}\right)\right)}{\left(1 + 0.4\left(\frac{1-x}{x}\right)\right)}\right]^{1/2}$	Slip	Multiple orientation including horizontal air-water Perform satisfactorily for $\alpha \leq 0.25$ $\alpha \geq 0.75$
		Homogeneous model-types		
16	Armand (1946)	$\alpha = 0.833\alpha_H$	Hom*	Horizontal air-water Perform moderately for $\alpha \leq 0.25$ and $0.50 \leq \alpha \leq 0.75$
17	Nishino and Yamazaki (1963)	$\alpha = 1 - \left(\frac{(1-x)}{x}\frac{\rho_G}{\rho_L}\alpha_H\right)^{0.5}$	Hom*	Unknown orientation Perform satisfactorily for $\alpha \geq 0.75$
18	Chisholm (1983)	$\alpha = \frac{\alpha_H}{\alpha_H + (1 - \alpha_H)^{0.5}}$	Hom*	Horizontal air-water Armand (1946) modified correlation Performed moderately for $\alpha \leq 0.25$ and satisfactory for $\alpha \geq 0.75$
19	Czop et al. (1994) *et al.* (1994)	$\alpha = -0.285 + 1.097\alpha_H$	Hom*	Helically coiled tube Air-water mixtures gas mass fractions from 0.04 to 0.6.
		Empirical model-types		
20	Huq and Loth (1992)	$\alpha = 1 - \frac{2(1 - x_g)^2}{1 - 2x + \left[1 + 4x(1-x)\left(\frac{\rho_L}{\rho_G} - 1\right)\right]^{0.5}}$	Slip	Unknown orientation Performed satisfactorily for $\alpha \leq 0.25$ $\alpha \geq 0.75$

Hom* - Homogeneous void fraction model types.

3. Test facility and methods

The experimental tests included in this study were performed on the two-phase rig located in the Process Systems Engineering Laboratory at Cranfield University UK. The process loop consists of a horizontal test pipe-route section, with an internal diameter of 0.05m, (2-in.). The 25 m long test section is divided into two sections: a 15 m long section and a 9 m long section upstream and downstream of the nozzle throat, respectively. A schematic of this facility is shown in figure 2.

In this work there is no low-pressure fluid, thus the low-pressure side is kept closed allowing the mixing-chamber to act as a void chamber. Under operation the void space undergoes a reduction of pressure because of the high-speed jet. Thereby, the total pressure drop can be estimated via the subtraction of the upstream absolute pressure (upstream nozzle throat) from the stagnant pressure of the vacuum chamber. The stagnant pressure in the vacuum chamber behaves inversely proportional to the power of the jet, which is a function of the motive pressure and mixture density.

However, the latter pertains under sub-critical flow conditions only, thus choking conditions are not met at the throat of the nozzle. When choking conditions are met, vibrations are present and initiate an intermittent jet behaviour. In this case, it is complex to correlate the total mass flow-rates directly via differential pressures.
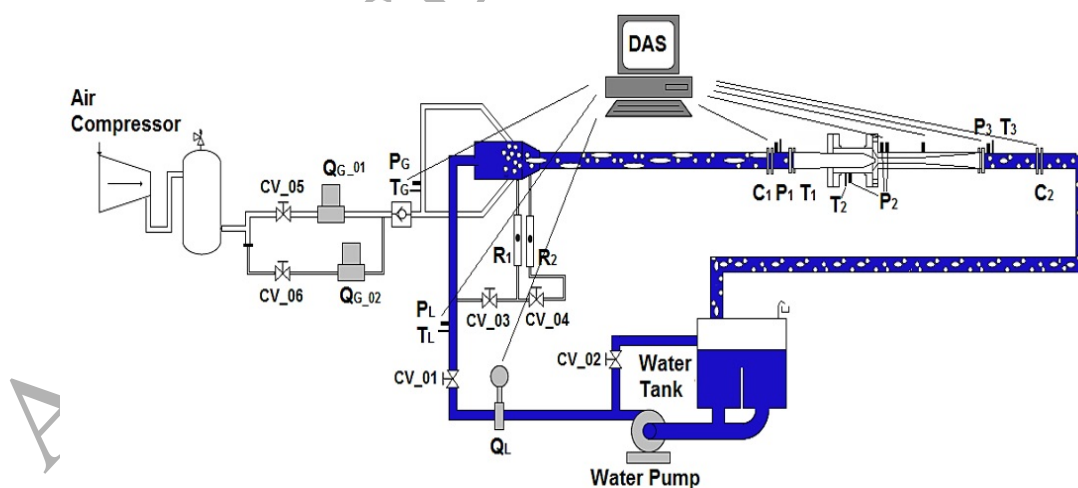

Figure 2: Schematic of the experimental test loop and data acquisition system.

Water was supplied from a 1.5 m³ storage tank via a HP centrifugal pump able to supply a maximum flow capacity of 2.4 lps at a pressure of 8 barg. The flow-rate of water was manually controlled via a combination of two globe valves, namely CV01 and CV02. It was measured by an Endress+Hauser® electromagnetic flowmeter, having a rangeability of 0-600 m³/hr, and within an uncertainty of +/- 1 % of FS.

Air was supplied by an in-place twin compressed air unit system consisting of two Atlas-Copco® compressors. Both compressors were controllable by a built-in Delta-V® system. The compressed air system had a maximum flow-rate of 1410 Sm³/hr - FAD at a pressure of 7.5 barg, and was controlled via a bank of two Rosemount® Mass Probar® flow meters of 1/2 inch and 1 inch diameter respectively. The smaller air flow meter measured the lower air flow-rate up to 150 Sm³/h, while the larger one metered the higher air flow-rate up to 4250 Sm³/h. Both meters have and uncertainty of +/- 1 % of FS.

In extreme flow conditions, thus when involving high gas volume fractions (GVFs), above 0.95 and low GVFs (below 0.1), the gas injection in the case of high liquid - low gas or the liquid injection in the case of high gas - low liquid, was performed via separate low range air flow meters for gas, or with a rotameter for liquid.

The air flow meter used comprised an Aalborg® thermal-type mass flow meter, having a range of 0-500 Slpm with a measurable uncertainty of +/- 5 % of FS. Multiple types of Key® rotameters were used to cover low liquid flow-rates ranging between 5-100 Slpm. All rotameters operated within an uncertainty of +/- 4 % of FS.

The mixing of the two phases was set to occur at a commingle point located 15 m far upstream of the nozzle-throat. The mixing point was configured to obtain the best homogeneous mixing via two-gas injection conduits connected to two separate gas-inlet ports fixed at a 60° angle to the (2-in) main pipe of the flowing water.

The test section in the ejector-like configuration included a Plexiglass body, which was geometrically designed to hold a convergent nozzle in place, while allowing a void space around this nozzle. The void space was used to measure the pressure of the high speed moving jet, i.e. a purely suction power resulting from the two-phase high-speed jet exiting the nozzle-throat. The described test piece is illustrated in figure 3.

Several sensors were installed in the test section to measure the performance parameters at local conditions where temperature, pressure and conductivity were recorded. A set of sensors
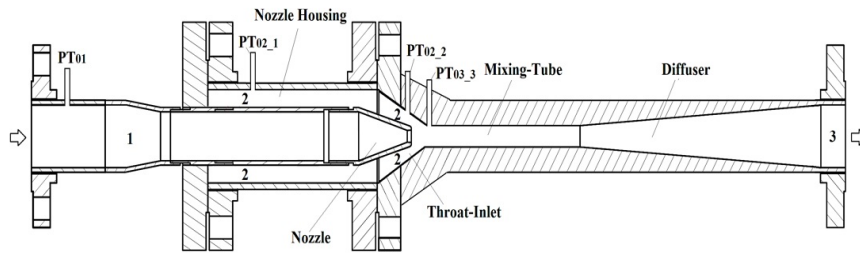
Figure 3: Cross-sectional view of the test piece used for conducted experiments.

(comprising a pressure transducer, a temperature probe and a set of conductivity rings), was installed at positions No.1 (upstream nozzle) and No. 3 (discharge position), while at position No.2 (within the nozzle housing and the throat-inlet), three pressure transducers were in place. The first pressure transducer 'PT02_1' recorded the pressure along the void space between the nozzle and the inner wall of the nozzle housing, the second transducer 'PT02_2' recorded the pressure at mid-way of the throat-inlet convergent portion. The third transducer 'PT02_3' recorded the pressure at the inlet of the mixing tube.

This procedure was performed to note any variance of the measured pressure at downstream positions, thus measurement of pressure at the vena-contracta and at the mixing tube inlet, the latter being at a position where the expansion of the jet occurs, thus causing portion of this jet to impinge on the curved wall. Additionally, the inclusion of multiple pressure tap-points in the downstream region of the nozzle also helped to determine the point where pressure recovery started to occur. The variance of the two-phase jet in the conical region is illustrated in figures 4(a) and 4(b).

It can be seen in figure 3 that the jet-coning profile widened up with the increase of gas in the system. It was noted that at high flow quality, the vena contracta at the throat-inlet and the mixing tube inlet vanishes. Moreover, a point was reached where a flow recirculation was present at the throat-inlet. All three pressure transducers recorded almost the same value for low GVFs, but differences gradually increased with the increase of GVFs.

The pressure at both throat-inlet 'PT02_2' and mixing tube inlet 'PT02_3' gradually changed from the stagnant pressure 'PT02_1' with the increase of gas content. This signifies that under such conditions, the pressure 'PT02_1' measured in the void chamber, maintains a true pressure as if it were still possible to get measurements in the vena contracta. All pressure sensors com-
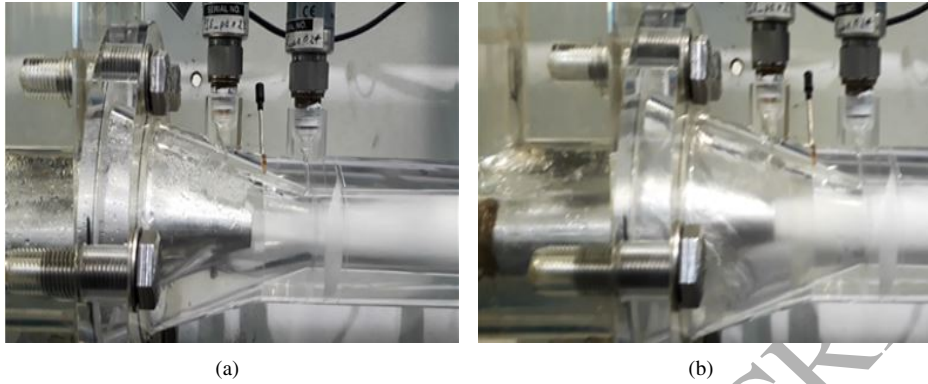
Figure 4: Two-phase flow jetting out from the nozzle throat at high speed; *(a)* two-phase jet at low GVFs, *(b)* two-phase jet at high GVFs.

prised Druck® pressure transducers, with variable ranges of 0-6 bara, 0-1 bara and 0-12 bara, and with an average uncertainty of +/- 0.15 % of FS. Temperatures were measured at the same locations via thermocouple type-k sensing devices.

Additionally, the gas void fraction was difficult to estimate via its defining expression:

$$\alpha = 1 - H_{\text{L}} \tag{22}$$

with H_{L} the liquid hold-up:

$$H_{\text{L}} = \frac{A_L}{A_L + A_G} \tag{23}$$

where A_L and A_G are the cross-sectional areas of the pipe occupied by liquid and gas respectively.

Both physicist and engineers have always found it difficult to directly estimate the area occupied by liquid and gas phases inside a multiphase stream. In this work, the method applied to measure the void fraction was to use a non-intrusive impedance technique via two pairs of conductance probes. This conductance methodology is a well-known and widely applicable non-expensive technique for the continuous measurement of void fractions / liquid hold-ups. Several authors have successfully used such measuring technique, see for instance Gregory and Mattar (1973), Rosehart et al. (1975), Tsochatzidis et al. (1992), Elkow and Rezkallah (1996), Song et al. (1998), Fossa et al. (2003) and Ko et al. (2015).

The rig-setup illustrated in figure 2 comprises two pieces of conductivity measuring devices. The first conductivity measuring device (C_1) is installed upstream of the HP nozzle, while the second conductivity measuring device (C_2) is located downstream of the discharge port of the JP device. Note that for this particular case, the conductivity measuring device (C_1) was the one used to estimate the HP fluid averaged void fraction. As illustrated in figure 5, this measuring device includes two measuring probes, probe (C_{1-a}) and (C_{1-b}).
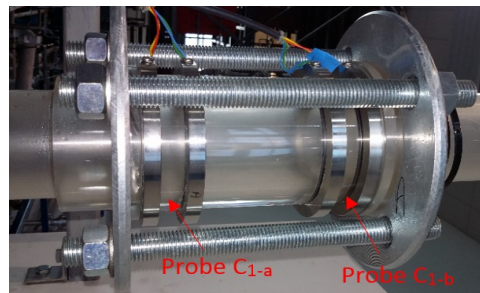
Figure 5: This work conductivity measuring device.

Each probe was used to calculate the change in electrical impedance between a pair of stainless-steel electrode; electrodes separated by the same two-phase flowing fluid. This flowing fluid acts as a dielectric material which enacts change in impedance, triggered as a result of the variation in void fraction.

A conductivity box was used, and which comprised an electrical circuit configuration as shown in figure 6. The illustrated circuit denotes a setup-configuration for one conductivity probe (having a pair of stainless steel electrodes). Such conductivity box was configured to output a voltage reading for each probe. The same voltages were real-time recorded via the Lab-View software.

Before running the experiments, the calibration of the conductivity probes was carried out in order to develop a relationship between the void fraction (of the mixture stream) in the conduit and the normalized output voltage. A very simple procedure was applied: (1) place the probes test-section (flanged at both ends) as shown in figure 6 on a flat table, (2) connect the probes to an electronic conductivity box feeding voltage signals into the LabView® software for data acquisition, (3) record the voltage reading when the conduit contains 100 % gas-air, (4) record the voltage reading when the conduit contains 100 % liquid-water, (5) empty and measure the volume of water via an Azlon 500 mL graduated cylinder, (6) refill with 100 % liquid-water, and
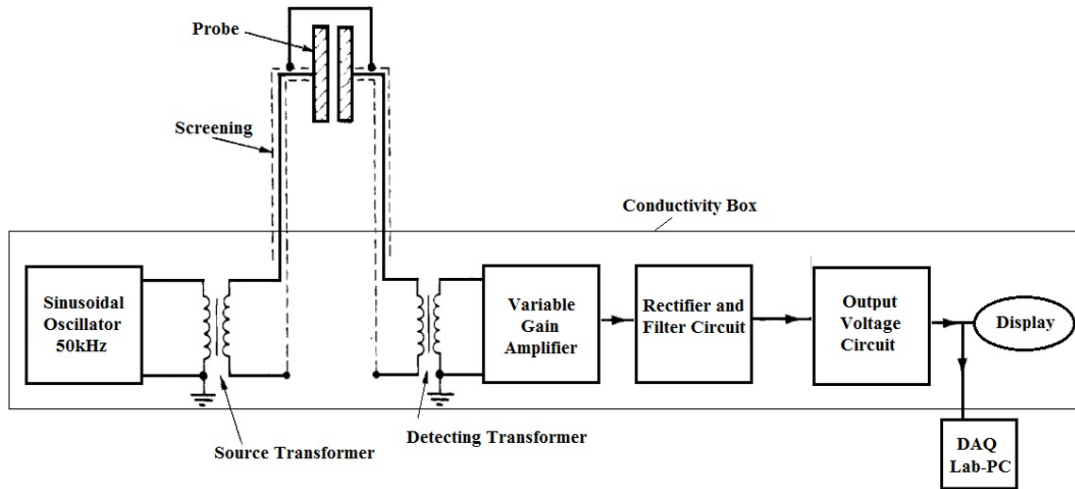
Figure 6: Schematic of an electrical circuit configuration of this work conductivity-box for 1 conductivity probe.

start taking voltage readings at consecutive steps, each involving a reduction of 5 % volume of liquid-water, and (7) plot the calibration curves (for each probe) as shown in figure 7.
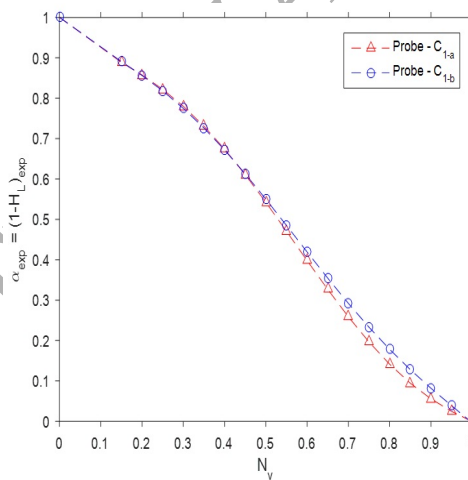

Figure 7: Void fraction α v.s. normalized voltage N_v for probe (C_{1-a}) and probe (C_{1-b}).

The following polynomial relationships obtained from the developed curves were then used to calculate the void fractions during the actual test conditions.

$$C_{1-a} = 1 - ((4.6992N_v{}^5) - (13.665N_v{}^4) + (12.78N_v{}^3) - (3.898N_v{}^2) + (1.0845N_v)$$
$$-(3.16246.10^-4)) \tag{24}$$

$$C_{1-b} = 1 - ((3.6065N_v{}^5) - (9.9958N_v{}^4) + (8.9583N_v{}^3) - (2.50N_v{}^2) + (0.9345N_v)$$
$$-(3.1446.10^-5)) \tag{25}$$

The normalized voltage N_v was calculated according to the following equation:

$$N_v = \frac{C_a - C_{Min}}{C_{Max} - C_{Min}} \tag{26}$$

where C_{Min} is the conductivity signal for single phase air flow (when the pipe is fully occupied by air), C_{Max} is the conductivity signal for single phase water flow (when the pipe is fully occupied by water) and C_a is the conductivity signal for air-water two-phase flow.

During the calibration process, it was estimated that the error in the void fraction measurement was ±0.5 mL (±2%). It is also important to state that the calibration was performed under stratified flow regime. Under actual conditions, bubble and slug flow patterns could lead to an increase of the uncertainty in the void fraction calculation. However, as the void fraction was averaged, the uncertainty remained within ±5%.

All measurements were acquired by a data acquisition card (DAQ) from National Instruments Inc® and via several custom-built signal conditioning units. The input data was managed via a developed program in LabView® (version 7). The developed program gathered all real-time data from all Data Acquisition System (DAS) hardware and converted the respective input voltage into engineering units. Tests were recorded with a scan rate of 20 scans per second for a duration of 120 seconds. The data was then exported into a custom-built database, where the 2400 readings per test were averaged into a single value for data analysis.

The test matrix adopted for the conducted two-phase (air-water) experiments is illustrated in figure 8, including a flow regime map proposed by Mandhane et al. (1974).

The flow regimes covered were within the bubble/elongated bubble and slug flow regimes for the case of high liquid - low gas, while stratified, wavy and slug flow regimes were covered
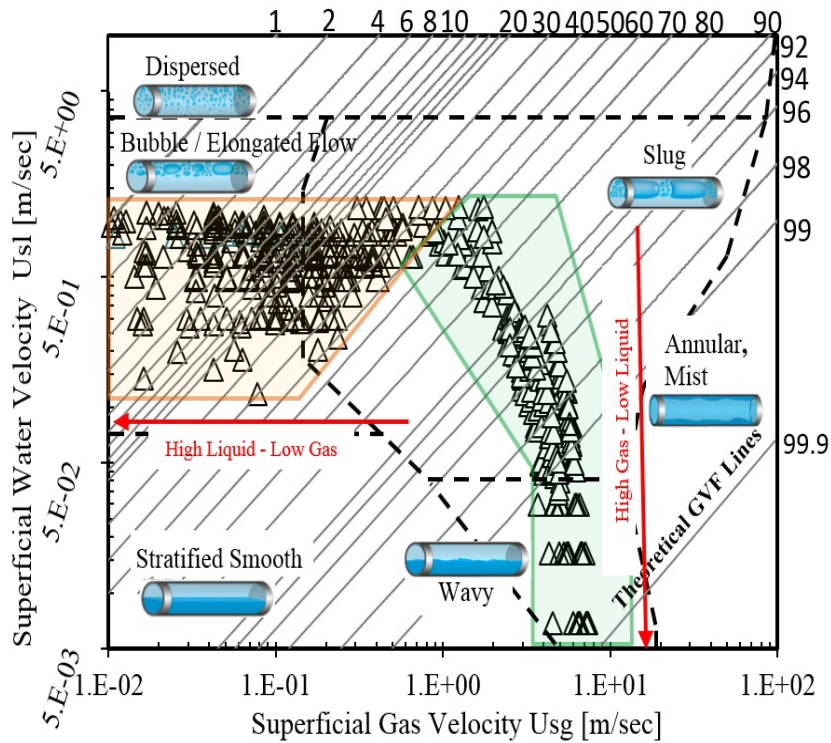
Figure 8: Test matrix overlaid on Mandhane et al. (1974) flow regime map, for superficial phase velocities calculated upstream the nozzle constriction.

for the case of high gas - low liquid flow combinations. Note that the obtained flow patterns displayed in the flow regime map in figure 8 include superficial gas and liquid velocities based on upstream conditions and not from the throat section. The flow regime upstream of the inlet section was also visually noted via a transparent test section.

4. Models formulation

4.1. The incompressible Bernoulli's continuity equation

A generic expression of the differential pressure flow equation can be derived from Bernoulli's relation. This expression can be used to calculate the total mass flow-rate of both single and two-phase flows.

Considering the schematic illustrated in figure 9, the fluid flows from a high-pressure zone (upstream of the nozzle throat), Pt.1, down to a relatively low-pressure zone (at and just down-

stream of the nozzle throat), Pt. 2. The conversion of energy, from the dominant pressure energy upstream of the nozzle, to the kinetic energy at the nozzle throat and close-by regions, can be equated via the Bernoulli continuity relationship:
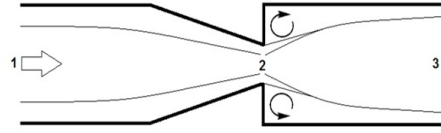

Figure 9: Fluid flow across test pipe-nozzle-pipe section.

$$P_1 + \tfrac{1}{2}\rho V_1^2 + \rho g h_1 = P_2 + \tfrac{1}{2}\rho V_2^2 + \rho g h_2 \tag{27}$$

where the pressure energy is given by P, while the potential and kinetic terms are expressed via the collective terms of $\rho g h$ and $\tfrac{1}{2}\rho V^2$ respectively. V is the speed of the flow, g the acceleration due to gravity, h the height against a common reference point and ρ the density. The subscripts 1 and 2 denote the upstream and throat/just downstream locations respectively.

As the tests were performed in a horizontal pipe section and with a relative small diameter (52.4 mm), the term accounting for potential energy is neglected on both sides of Bernoulli's equation.

Thereby equation (27) reduces to:

$$\Delta P_{tot} = P_1 - P_2 = \tfrac{1}{2}\rho V_2^2 - \tfrac{1}{2}\rho V_1^2 \tag{28}$$

Equation (28) signifies that the total pressure loss , ΔP_{tot}, is only function of the pressure loss due to acceleration. Thus, this expression neglects all irrecoverable pressure loss components, mainly involving losses due to friction from surface roughness and flow obstruction surfaces causing vortex detachments, contraction, compressibility including the variance of mixture density, expansion, elevation and phase slippage.

Equation (28) can therefore be re-written in terms of the five pressure loss components:

$$\Delta P_{tot} = P_1 - P_2 = [\, P_{acceleration_{loss}} + \\ P_{elevation_{loss}} + P_{friction_{loss}}] \tag{29}$$

where $\Delta P_{friction_{loss}}$ is a general term which comprises all compressibility losses such as both

contraction and expansion losses, and phase slip losses. Note that the pressure loss due to acceleration $\Delta P_{acceleration_{loss}}$ is assumed a recovered loss, and for this study, elevation losses do not apply. In addition, based on the above divisions responsible for pressure losses, it is a standard practice that in case of single-phase fluids a correction factor is applied either directly to the pressure drop or if not, the correction is managed via a discharge loss coefficient which accounts for all irreversible losses, mainly comprising friction and contraction effects. Thus equation (28) becomes:

$$\Delta P_{tot} = P_1 - P_2 = \tfrac{1}{2}\rho[V_2^2 - V_1^2] + (\Delta P_f) \tag{30}$$

where ΔP_f denotes pressure drop attributed to frictional losses. Thus equation (30) can be written as:

$$V_2 = \sqrt{\frac{2[\Delta P_{tot} - (\Delta P_f)]}{\rho\left(1 - \frac{d^4}{D^4}\right)}} \tag{31}$$

where d, and D are the diameters of the nozzle throat and upstream pipe respectively.

The mass conservation can be written as:

$$\dot{M}_{mix} = \rho A_2 V_2 \tag{32}$$

with $\dot{M}_{mix}$ the total mass flow-rate and A_2 the nozzle throat cross-sectional area.

ΔP_{tot} includes frictional losses which are unknown, and a discharge coefficient C_d is used, which is the most common parameter which accounts for the irrecoverable losses of a geometrical device under certain flow conditions. Thus, substituting (31) in equation (32), and multiplying by the coefficient of discharge C_d, equation (33) can be written. This equation is considered as a general form used to calculate the total mass flow-rate of an incompressible fluid.

$$\dot{M}_{mix} = \frac{C_d A_2 \sqrt{2\rho\Delta P_{LO}}}{\sqrt{1 - B^4}} \tag{33}$$

where ΔP_{LO} denotes the pressure drop for the case having liquid-water only, and $B = \left(\frac{d_n}{D_p}\right)$, with D_p and d_n the diameters of the nozzle inlet and throat respectively.

For the results presented in this paper, including two-phase flow conditions, the losses applicable to the experimental set-up were accounted for via a two-phase pressure drop multiplier

Φ^2_{lo}, which is considered a collective pressure loss factor parameter. This two-phase pressure drop multiplier is based on the same concept as for the frictional pressure drop multiplier applicable to calculate pressure loss in conduits.

Multiplying Φ^2_{lo} and the total pressure drop of the two-phase flow ΔP_{mix} (treated as if it were a single-phase pressure drop) and substituting both expressions in the general equation (33), equation (34) which is a modified equation capable of estimating the total mass flow-rate of two-phase compressible (water-air) mixtures can be established:

$$\dot{M}_{mix} = \frac{C_d * A_2 * \sqrt{2\rho\Delta P_{mix}\Phi^2_{LO}}}{\sqrt{1-B^4}} \tag{34}$$

4.1.1. Single-phase flow through Nozzle

In the case of a single-phase flow (100 % water), equation (34) is used with a value $\Phi^2_{LO} = 1$, and a constant value $C_d = 0.9$. The value of C_d constitutes an average value obtained from calibration tests involving 100 % water. Ultimately, equation (34) becomes:

$$\dot{M}_{liq} = \frac{C_d A_2 \sqrt{2\rho_{liq}\Delta P_{liq}}}{\sqrt{1-B^4}} \tag{35}$$

4.1.2. Two-phase flow through Nozzle

When considering a two-phase flow, the value of Φ^2_{LO} in equation (34) is not equal to 1. Hence assuming the same values of C_d and ρ as those used in the case of 100 % water, and substituting the values of $\dot{M}_{mix}$ and ΔP_{mix} directly from the generated dataset, the corresponding values of Φ^2_{LO} can be estimated via the following expression:

$$\Phi^2_{LO} = \left[\frac{\dot{M}_{mix}}{C_d \, A_T}\right]^2 \left(\frac{(1-B^4)}{(2\rho_{liq}\Delta P_{mix})}\right) \tag{36}$$

Note that Φ^2_{LO}, is changed to $\Phi^2_{LO_{HL}}$ and $\Phi^2_{LO_{HG}}$ for cases of high liquid - low gas and high gas - low liquid flows respectively.

4.2. Two-phase flow through nozzle for Case A-high liquid-low gas

Case A describes the method used for the developed two-phase pressure-drop multiplier and discharge loss coefficient correlation, valid in the region of high liquid - low gas fluid compositions. The following step by step procedure was applied:

- Equation (36) was used to calculate values of the Φ_{LO}^2 for 175 data points. These 175 data points constitute half the experimental data set which includes two-phase flow combinations having $\alpha < 0.55$.

- Φ_{LO}^2 was compared with the 5 models described previously: HEM - Green and Perry (1973)), Simpson et al. (1983), Chisholm (1983), Morris (1985), and Alimonti et al. (2010).

- Based on the results, a tuning parameter was necessary to compensate for losses attributed to different design geometry.

Results showed a high similarity between this work and the Morris two-phase multipliers. Given that C_d was kept constant, the applied tuning was fully integrated in Φ_{lo}^2. The modified two-phase multiplier can be written as a product of two two-phase multipliers:

$$\Phi_{LO_{HL}}^2 = \Phi_{LO_{Morris}}^2 \ \Phi_{lo}^2 \tag{37}$$

where $\Phi_{LO_{HL}}^2$ refers to the pressure drop multiplier provided by equation (36), $\Phi_{LO_{Morris}}^2$ refers to the pressure drop multiplier estimated by the correlation proposed by Morris (1985), while Φ_{lo}^2 is an added two-phase multiplier which accounts for the variance of the discharge coefficient for multiphase flows $C_{d_{multi}}$ and an additional tuning parameter; both are function of the two-phase flow quality x, matching Morris' expression.

The expanded version of equation (37) gives:

$$\Phi_{LO_{HL}}^2 = \Phi_{LO_{Morris}}^2 \ (\Psi_1 + \Psi_2) \tag{38}$$

where Ψ_1 constitutes the variance of $C_{d_{multi}}$, with an increase flow quality x, and Ψ_2 is a tuning value. Both Ψ_1 and Ψ_2 are obtained from experimental calibration given in figure 10(b) and figure 13 respectively.

It is found that the relationship between $C_{d_{multi}}$ and the flow quality x, obeys a polynomial function of degree 3, while the relationship for the tuning value Ψ_2 against the flow quality x obeys a power law function.

$$\Psi_1 = Ax^3 + Bx^2 + Cx + D \tag{39}$$

and

$$\Psi_2 = Ex^F \tag{40}$$

where *A, B, C, D, E* and *F* are constants generated from a linear regression, see table 3. Substituting Ψ_1 and Ψ_2 in equation (38) gives:

$$\Phi^2_{LO_{HL}} = \Phi^2_{LO_{Morris}} \left(\left(Ax^3 + Bx^2 + Cx + D \right) - Ex^F \right) \tag{41}$$

Thus, the proposed correlation satisfies the following relationship:

$$\Phi^2_{LO_{HL}} = \Phi^2_{LO_{Morris}} \Phi^2_{lo} = \left[\frac{\dot{M}_{mix}}{C_{d_{liq}} A_T} \right]^2 \left(\frac{\left(1-B^4\right)}{\left(2\rho_{liq}\Delta P_{mix}\right)} \right) = \tag{42}$$
$$f(C_{d_{mulit}}, \rho_g, \rho_l, x, S)$$

The derived two-phase pressure-drop multiplier correlation proved valid for the convergent nozzle-type under consideration, and holds for void fractions up to 0.5. Eventually, the general total mass flow equation given in equation (34) resolves to equation (43). Note that $\dot{M}_{HL}$ refers to the high liquid - low gas flow region.

$$\dot{M}_{HL} = \frac{C_{d_{liq}} A_T \sqrt{2\rho_{liq}\Delta P_{mix}\Phi^2_{LO_{HL}}}}{\sqrt{1-B^4}} \tag{43}$$

Table 3: Coefficient values for the derived $\Phi^2_{LO_{HL}}$ correlation - high liquid - low gas.

Empirical Coefficient Values					
A	B	C	D	E	F
-635076	11571	-80	0.96	1.2	0.35

This method (for Case A), including the high liquid -low gas region, is compared against several other two-phase pressure drop correlations and against the semi-empirical Non-Equilibrium Model (HNE-DS) developed by Diener and Schmidt (2004).

4.3. Two-phase flow through nozzle for Case B - high gas - low liquid

Case B includes two distinctive methodologies, one being similar to the one applied in Case A, and the other one involving the Mach number. The proposed correlations are valid in regions characterised by high gas - low liquid fluid compositions.

4.3.1. Case B (Method-01): high gas - low liquid

This case considers the variance of the discharge coefficient C_d (from single-phase to multi-phase flow conditions), separately from the developed two-phase pressure drop multiplier Φ^2_{LO}. $C_{d_{liq}}$ was initially assigned a value of 1, and subsequently assessed after an expression of the two-phase multiplier was developed. This case however slightly differs from Case A (for high liquid - low gas fluid), as the latter attributes the variance of the discharge coefficient directly in the correlation developed for the two-phase multiplier.

For this method, the following step by step procedure was applied:

- Equation (36) was used to calculate values of Φ^2_{LO}, including 80 data points. These data points involved two-phase test mixtures, with void fractions $\alpha > 0.75$.

- A comparison of Φ^2_{LO} with the models from HEM Green and Perry (1973), Simpson et al. (1983), Chisholm (1983), Morris (1985), and Alimonti et al. (2010) was performed.

Results revealed that there is no direct relationship between the two-phase multiplier $\Phi^2_{LO\_HG}$ and the void fraction α. The plotted data in figure 19 demonstrates high scattering, which kept on increasing with the increase of void fractions.

To develop a relationship between the two-phase multiplier $\Phi^2_{LO\_HG}$ and the void fraction α, the Mach number Ma was taken into consideration. The set of data points was then sorted in segregated ranges of Mach numbers, covering $0 < Ma < 1$. The objective of using the Mach number was to introduce a fundamental parameter which accounts for compressibility effects, when high gas is present in two-phase flows. The Mach number is a ratio between the actual velocity v in (m/s) of the multiphase mixture to the sonic speed c in (m/s) of the same mixture and at same pressure conditions.

$$Ma = \frac{v}{c} \tag{44}$$

The speed of the multiphase mixture was established with the following equation:

$$\dot{M}_{mix} = \rho_e * A_t * v_{mix} \tag{45}$$

where $\dot{M}_{mix}$ is the actual total flow-rate of the mixture in (Kg/s), ρ_e is the momentum density of the mixture in (kg/m³), while v_{mix} is the velocity in (m/s) of the mixture flowing through the

nozzle throat.

Equation (45) considers the momentum mixture density. As the speed of gas is much higher than the speed of liquid water at the nozzle throat, phase slippage should be accounted for.

$$\frac{1}{\rho_e} = \frac{x_G}{\rho_G} + S_{ch}\frac{x_L}{\rho_L}\left(x_G + \frac{x_L}{S_{ch}}\right) \tag{46}$$

where S_{ch} is the slip ratio, provided by the Chisholm (1983) correlation given in equation (10), x_G is the flow quality and $x_L = (1 - x_G)$ is the fraction of liquid (water). Thus x_G is:

$$x_G = \left[\frac{\dot{m}_G}{\dot{m}_G + \dot{m}_L}\right] \tag{47}$$

The speed of sound in the two-phase mixture was calculated with the so called "frozen two-phase sonic velocity" model, expressed as:

$$c = \left[\frac{d\rho}{dp}\right]^{(-1/2)} \tag{48}$$

The two-phase mixture density ρ_m, is estimated by the following equation:

$$\rho_m = \alpha\frac{1}{v_G} + (1 - \alpha)\frac{1}{v_L} \tag{49}$$

where α gives the void fraction, thus the (gas portion) of the two-phase flow, v_L and v_G denote the specific volume of liquid and gas phases respectively.

Thus α is expressed by:

$$\alpha = \left[1 + \left(\frac{1-x_G}{x_G}\right)S\frac{v_L}{v_G}\right]^{-1} \tag{50}$$

where S denotes the slip between superficial velocities of gas and liquid and is calculated either by the Chisholm correlation in equation (10), or the Simpson correlation, equation (3). Thus, the slip varies according to the Martinelli parameter:

$$S = \begin{cases} S_{Chisholm} & - \text{ low quality} - X > 1 \\ S_{Simpson} & - \text{ high quality} - X < 1 \end{cases} \tag{51}$$

where X as the Martinelli parameter estimated by the following equation

$$\chi = \frac{1-x_G}{x_G}\left(\frac{V_L}{V_G}\right)^{1/2} \tag{52}$$

with V_L and V_G the superficial velocities of liquid and gas respectively.

If no phase change takes place, neglecting the two-phase slip dependence on pressure, and differentiating equation (41) lead to an equation expressing the variance of the void fraction with pressure:

$$\frac{d\alpha}{dp} = \alpha\,(1-\alpha)\,v_L\frac{dv_L}{dp} - \alpha\,(1-\alpha)\,v_G\frac{dv_G}{dp} \tag{53}$$

Combining equations (47), (48), (49), and (50), the sonic velocity is calculated as follows:

$$c = \left[\left(\alpha^2 + \alpha\,(1-\alpha)\,\frac{v_G}{v_L}\right)\frac{dv_G}{dp} + \left((1-\alpha)^2 + \alpha\,(1-\alpha)\,\frac{v_L}{v_G}\right)\frac{dv_L}{dp}\right]^{-1/2} \tag{54}$$

Solving and simplifying the above relationship leads to:

$$c = \left[\frac{\alpha v_G}{v_m c_G^2} + \frac{(1-\alpha)v_L}{v_m c_L^2}\right]^{-1/2} \tag{55}$$

where c_L and c_G denote the speed of sound in pure water and pure air respectively.

Although α can be calculated from equations (50), (51) and (52), yet the experimental void fraction α was used in equation (55) as described previously in the test facility and methods section. This approach has been initially used to reduce errors and has been applied before the validation against available correlations was performed.

The two-phase correlation covering the high gas - low liquid region with $\alpha \geq 0.75$ obeys a polynomial function of degree 3:

$$\Phi^2_{lo_{mod\_HG}} = \left(A\alpha^3 - B\alpha^2 + C\alpha - D\right) \tag{56}$$

where *A, B, C,* and *D,* are coefficients written in table 4.

The above equations along with their respective Mach numbers show that the estimated two-phase pressure drops match the measured values within a 10 % maximum error, see figure 23(a)

As initially stated, the value of the discharge coefficient $C_{d_{liq}}$ was found to increase slightly above 1 and the Mach number to tend to 1. Another relationship was developed to account for this variance. Theoretically, the value of $C_{d_{liq}}$ should not exceed unity, but in this case $C_{d_{Multi\_HG}}$

Table 4: Coefficient values for the derived $\Phi^2_{lo_{mod}}$ correlation - high gas - low liquid.

Mach No.	Coefficient Values			
	A	B	C	D
$[0 - 0.2]$	87186	217273	180135	49659
$[0.2 - 0.3]$	101943	252587	208375	57200
$[0.3 - 0.4]$	109468	270272	222609	61137
$[0.5 - 0.6]$	91549	221057	177905	47689
$[0.7 - 0.8]$	133872	332338	275401	76147
$[0.9 - < 1.0]$	208754	525082	440619	123307

absorbs a tuning parameter in the form of a direct multiple of the initial value of $C_{d_{liq}}$. The calibration equation is given by:

$$C_{d_{Multi\_HG}} = C_{d_{liq}} * I \qquad (57)$$

where $C_{d_{liq}} = 1$, and I is a calibration coefficient.

The final relationship is given by;

$$C_{d_{Multi\_HG}} = \left(E Ma^2 + F Ma + G \right) \qquad (58)$$

where the coefficients E, F and G, are assigned constant values of 0.154, 0.1496 and 0.973 respectively. Thus, the proposed correlation satisfies the following relationship:

$$\Phi^2_{LO_{HG}} = \left(A\alpha^3 - B\alpha^2 + C\alpha - D \right) = \left[\frac{\dot{M}_{multi\_HG}}{\left(C_{d_{liq}} * I\right) * A_T} \right]^2 \left(\frac{(1-B^4)}{(2\rho_{liq}\Delta P_{mix})} \right) = f(Ma, \alpha) \qquad (59)$$

The derived two-phase pressure drop multiplier correlation holds for void fractions ≥ 0.75. The general total mass flow equation given in equation (34) resolves to equation (60) as illustrated hereunder. Note that $\dot{M}_{HG}$ refers to the high liquid - low gas flow region.

$$\dot{M}_{HG} = \frac{C_{d_{Multi\_HG}} * A_T * \sqrt{2 * \rho_{liq} * \Delta P_{mix} * \Phi^2_{LO_{HG}}}}{\sqrt{1-B^4}} \qquad (60)$$

4.3.2. Case B (Method-02): high gas - low liquid

For this case, the two-phase flow correlation Φ^2_{LO} absorbs all pressure losses for the two-phase high gas – low liquid fluid. Such losses are due to irreversible energy losses of multi-phase discharge loss coefficients including friction and contraction effects, and two-phase fluid

compressibility effects. Besides, the two-phase multiplier accounts for the significant change in density (lower density for water and air mixture flows). This substantial variance of density made the two-phase multiplier susceptible for scattering, thus a tuning parameter (in terms of void fraction) was added to reduce the overall error. The procedure adopted was the following one:

- Equation (34) was used to calculate values of Φ^2_{LO}, including 80 data points. The considered data points involved two-phase test mixtures with void fractions $\alpha \geq 0.75$.

The developed trend-line, satisfied a polynomial relationship of degree 2, given by:

$$\Phi^2_{LO_{HG\_org}} = A\alpha^2 + B\alpha + C = \Psi_1 \tag{61}$$

where $\Phi^2_{LO_{HG\_org}}$ refers to the original frictional pressure drop multiplier, hence not yet modified, and coefficients *A, B, C,* are constants generated from a linear regression, see table 5.

- Tuning was required to smooth the scattered data points, hence fit data close to the developed trend-line.

The modified $\Phi^2_{LO_{HG}}$ in equation (63) comprises the product of Ψ_1 provided by the original relationship in equation (61), and Ψ_2, which includes a numerical variable obtained from the calibration which obeys a power law function in terms of void fraction α:

$$\Psi_2 = D\alpha^E \tag{62}$$

where *D* and *E* are constants generated from a linear regression given in table 5.

Ultimately the full relationship is given by:

$$\Phi^2_{LO_{HG}} = (\Psi_1 + \Psi_2) \tag{63}$$

Hence, substituting for Ψ_1 and Ψ_2 in equation (63), gives:

$$\Phi^2_{LO_{HG}} = \left(\left(A\alpha^2 + B\alpha + C \right) * D\alpha^E \right) \tag{64}$$

Furthermore, for an easier use of the above correlation (developed from two separate relationships) one expression was written, obeying a polynomial function of degree 2:

$$\Phi^2_{LO_{HG}} = \left(F\alpha^2 + G\alpha + H\right) \tag{65}$$

where F, G and H are constants generated from a linear regression given in table 5.

Thus, the proposed correlation satisfies the following relationship:

$$\Phi^2_{LO_{HG}} = \left(F\alpha^2 + G\alpha + H\right) = \left[\frac{\dot{M}_{mix}}{C_{d_{liq}} * A_T}\right]^2 \left(\frac{\left(1-B^4\right)}{\left(2\rho_{liq}\varDelta P_{mix}\right)}\right) = \\ f\left(\rho_g, \rho_l, \alpha, S\right) \tag{66}$$

The derived two-phase pressure drop multiplier correlation proved valid for the convergent nozzle-type under consideration, and holds for void fractions above 0.75. The general total mass flow equation given in equation (34) resolves to equation (67).

$$\dot{M}_{HG} = \frac{C_{d_{liq}} * A_T * \sqrt{2*\rho_{liq}*\varDelta P_{mix}* \Phi^2_{LO_{HG}}}}{\sqrt{1-B^4}} \tag{67}$$

Table 5: Coefficient values for the derived $\Phi^2_{LO_{HG}}$ - high gas - low liquid correlation.

Empirical Coefficient Values							
A	B	C	D	E	F	G	H
2.61	-5.09	2.49	0.87	0.327	1.992	-3.913	9.124

The described methods in Case B for the high gas - low liquid case will be compared with the semi-empirical Non-Equilibrium Model (HNE-DS) developed by Diener and Schmidt (2004) in the next section.

5. Results and Discussion

5.1. Case A-01 - high liquid - low gas

The results of the calibration tests of the 100 % liquid case and the two-phase cases are illustrated in figures 10(a) and 10(b) respectively.

Under two-phase flow conditions, the coefficient of discharge $C_{d_{liq}}$ decreases significantly with the increase of quality. A significant decrease is noted at a reference vapour quality of 0.01, resulting in a $C_{d_{mp}}$ of 0.65. A trend-line is drawn and equated within the resulted non-linear behaviour. This provides an equation which accounts for such effect and can be used in the developed two-phase multiplier model.
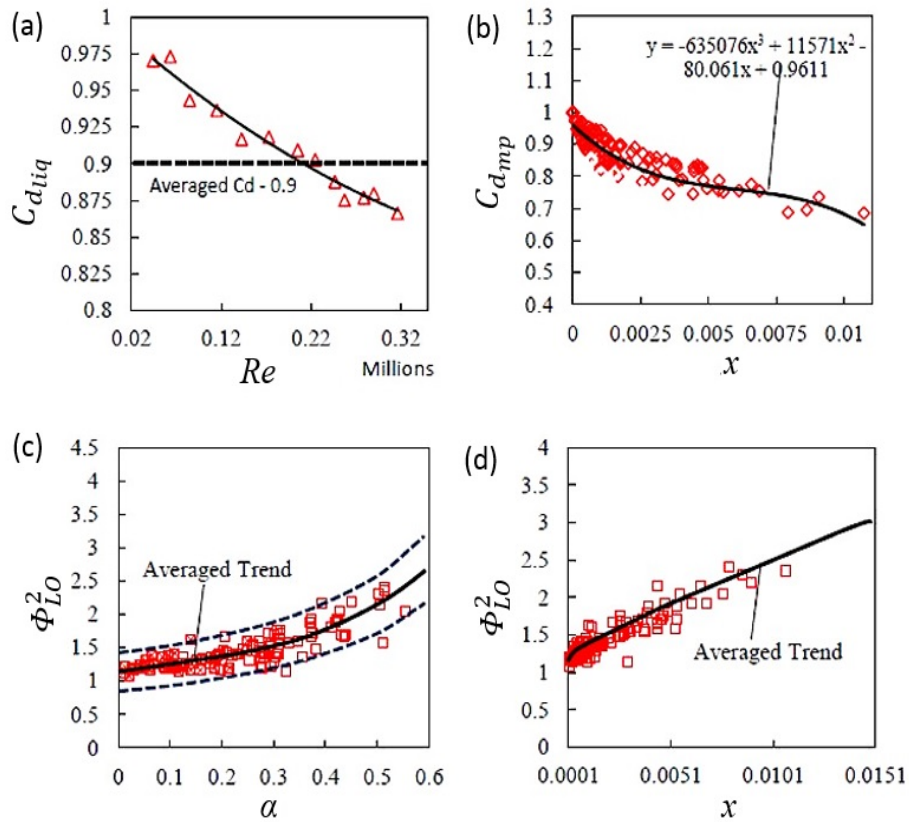
Figure 10: (*a*) Reynolds number *Re* v.s. nozzle discharge coefficient *Cd_liq* for 100 % liquid calibration tests; (*b*) two-phase flow vapour quality *x*, for $x \leq 0.012$, v.s. nozzle discharge coefficient *Cd_mp*; (*c*) void fraction α, for $\alpha \leq 0.55$, v.s. two-phase flow multiplier Φ_{LO}^2; (*d*) flow vapour quality *x*, for $x \leq 0.012$, v.s. two-phase flow multiplier Φ_{LO}^2.

Figures 10(c) and 10(d) shows the behaviour of the two-phase multiplier Φ_{LO}^2 (not modified) v.s. the void fraction α and the flow vapour quality *x*. An averaged trend-line is drawn within both populated plots.

Figure 11 show a comparison between the behaviour of the two-phase multiplier in this work (without-correction), the Homogeneous model (HEM), and models proposed by Chisholm (1983), Morris (1985), Simpson et al. (1983) and Alimonti et al. (2010). Results mostly follow a curvilinear behaviour. The averaged trend-line of this work multiplier, as previously displayed in figure 10(c), showed high similarity to the Morris (1985) model.

Figure 12 shows clearly that Morris' results share the closest behaviour with the present work. However, at this stage the work multiplier needs calibration and tuning to: (1) fit more
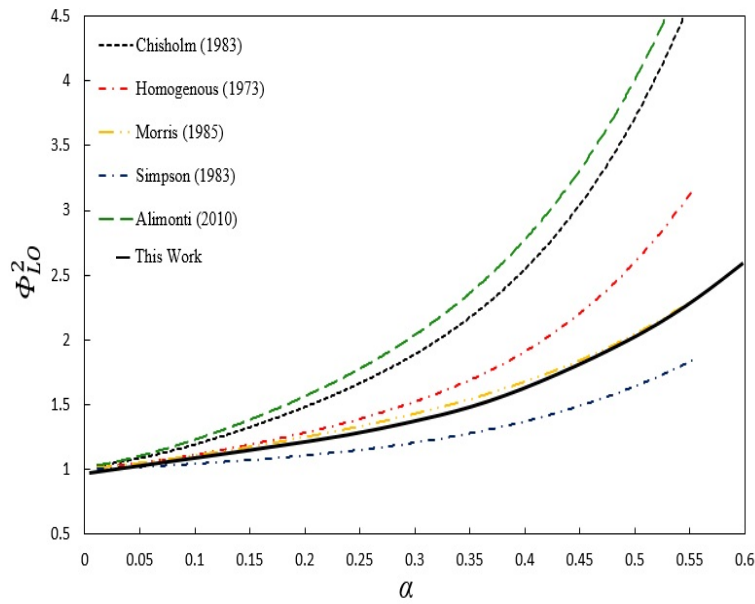
Figure 11: Void fraction for $\alpha \leq 0.55$, v.s. pressure drop multiplier Φ_{ref}, comparing this work behaviour (without-correction) against five other two-phase multiplier correlations.

data on the averaged trend-line in figure 10(c), and (2) account for irreversible losses, mainly due to friction.
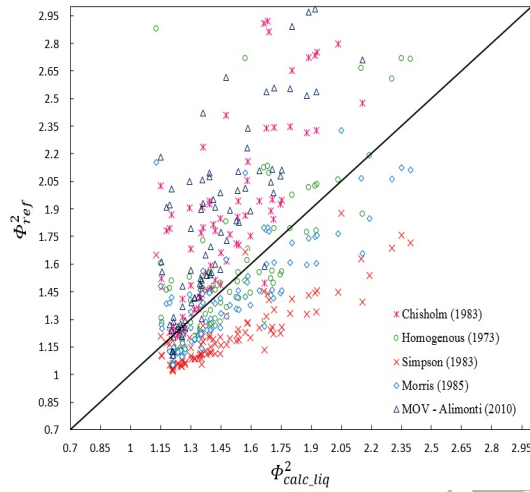
Figure 12: Calculated (without correction) $\Phi^2_{calc_{liq}}$ 2 v.s. reference two-phase multiplier Φ_{ref} models.

Figure 13 shows a power law behaviour that exists for the defined value Ψ_2 and the flow quality x. It is noted that the tuning value Ψ_2 increases with an increase in quality x. This tuning parameter based correlation predicts total two-phase mass flow rates with less than 10 % error.
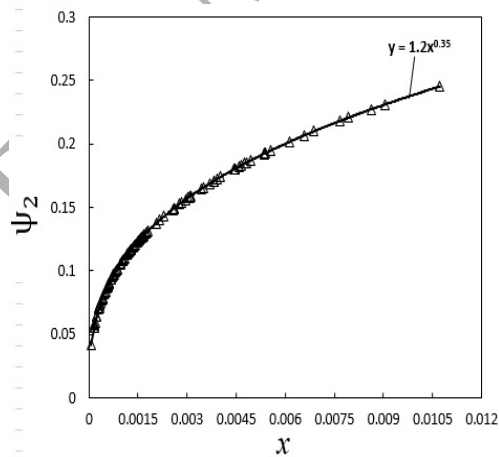
Figure 13: Flow quality x v.s. tuning parameter ψ_2.

Figure 14(a) shows the effect of the calibration via the tuning factor Ψ_2. The performed corrections made the measured and calculated mass flow-rates to agree within a +/- 10 % error band. Moreover, figure 14(b) illustrates the combined effect within the modified two-phase multiplier
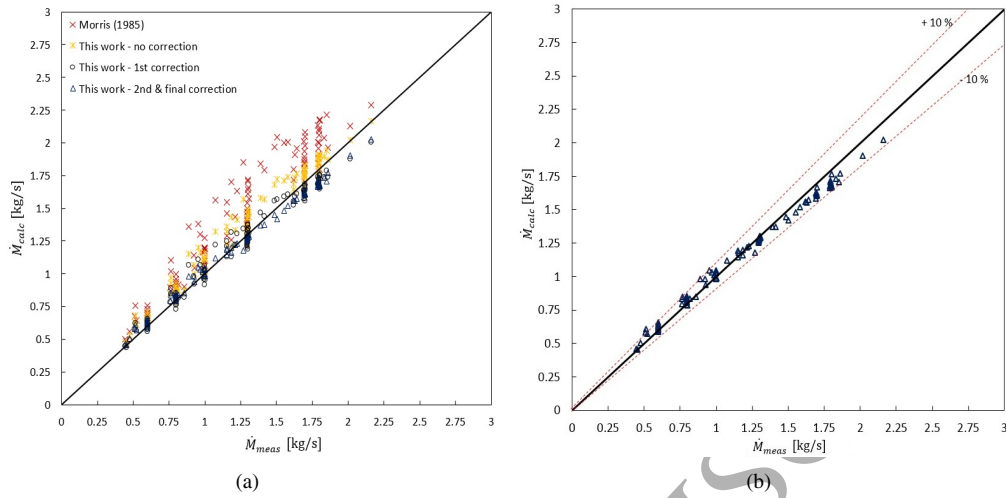
Figure 14: *(a)* Measured v.s. calculated total mass flow-rate for Morris correlation, this work (without correction), this work (1st correction) - including the effect of Cd_multi, and this work (2nd correction) - including the effect of the tuning parameter ψ_2, and *(b)* Measured v.s. calculated total mass flow-rates for the developed two-phase multiplier with final correction Φ^2_{HL}.

via the tuning parameter Ψ_2 and the calibration of Cd_mp, denoted Ψ_1.

Besides the comparison of results of pressure-drop multipliers only, figure 15 shows a comparison between this work two-phase pressure drop multiplier correlation and the semi-empirical HEM-DS method. As noted by Diener and Schmidt (2004), this model tends to be accurate when the stagnation flow quality x is above 0.15. Thus, this particular case has just shown that for two-phase flows having a maximum quality of 0.012 (thus much less than 0.15), extensive scattering is obtained.

In this case, it could be stated that the HEM-DS model automatically reduced to the HEM (w) model, since no water turned into vapour, and the boiling delay factor N is 0.

Results using the same HEM-DS method will also be compared for fluids in the high gas - low liquid region, in Section 5.3.2.
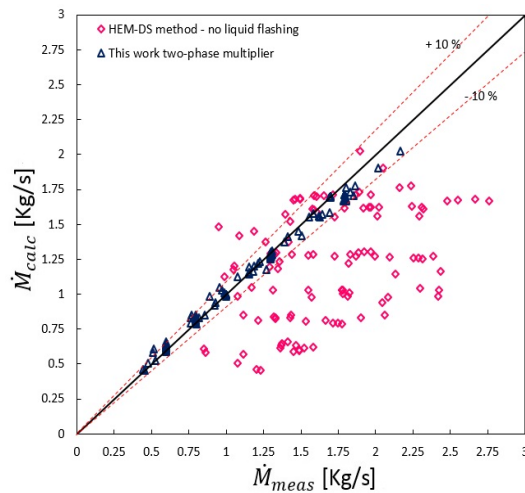
Figure 15: A comparison for measured v.s. calculated total mass flow-rates for this work high liquid - low gas empirical correlation and semi-empirical HEM-DS method.

5.2. *Case A-02 - Comparison between Various Geometric Configurations*

A comparison of the resulting two-phase pressure drop multiplier for the case of high liquid - low gas fluid compositions, i.e. for two-phase fluids of void fractions $\alpha \leq 0.55$, was performed. Results were plotted against six other referenced two-phase pressure drop multiplier correlations. Each of the six correlations included a geometrical flow configuration.

The evaluation comprised (1) this work configuration consisting of a convergent nozzle of negligible throat thickness, (2) a single-orifice plate, (3) a gate valve, (4) a globe valve and (5) a Venturi-body whose geometrical configuration was modified to assess three different throat lengths: (5-a) a short throat of 0.36 *d*, (5-b) a medium-throat of 1.16 *d*, and (5-c) a long-throat of 4.16 *d* respectively, with *d* the throat diameter. Figure 16 shows a schematic representation of the referred geometrical configurations.

In the case of the orifice plate, globe valve and gate valve, the data reported by Fairhurst (1983) were also validated against the compressible flow model derived by McNeil (2000). The respective results and comparison between models resulted in a high agreement. The referenced data for the Venturi-body was based on the work of Silva et al. (1991), which included a model that accounted for slip via the Chisholm (1983) slip correlations. Additionally, all referenced models were applied for two-phase fluids of water-air mixtures, and experiments were performed at relative low pressures (< 10 bara). Those operating conditions were therefore identical to those
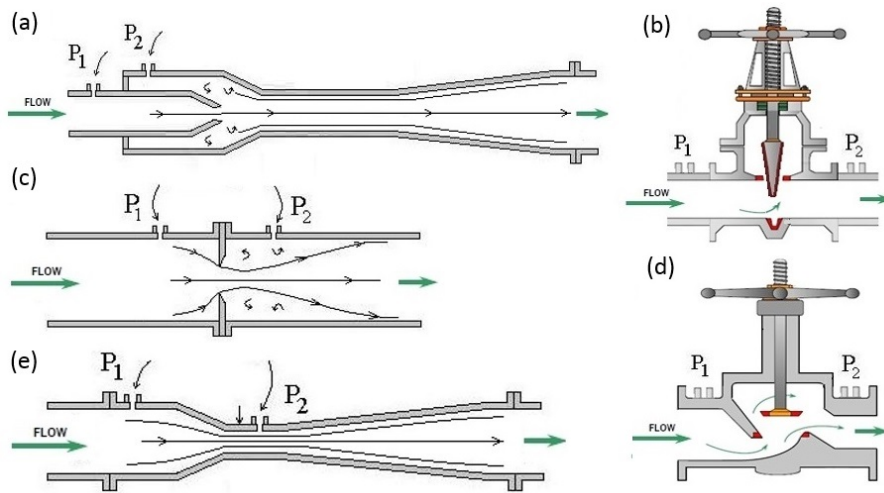
Figure 16: Devices included in this study comprising of different geometric configurations, *(a)* this work jet pump-like design, *(b)* gate valve, *(c)* single orifice plate, *(d)* globe valve, and *(e)* Venturi-body.

encountered in this work.

Figure 17 illustrates the behaviour of the two-phase frictional pressure drop multiplier for all seven geometric configurations. The two-phase multiplier is a function of the loss mechanism factors attributed to a specific geometric configuration. This study highlights two types of loss factors.

The first loss factor, considered to be the dominant one, involves losses due to compressibility effects. A fluid mixture comprising two phases such as water and air behaves differently from liquid-water only and tends to show an increase of variation with the increase of the secondary compressible phase (air). Note that this most dominant factor it also the most complex to estimate in flows showing high quality.

The second loss factor mainly captures all frictional losses which may be attributed to (1) a variance of flow direction such as experienced in globe valves, (2) a sudden expansion for non-axisymmetric flow paths such as for gate valves, (3) an interference between multiple streams of flow in case of flow paths in multiple orifices or multiple flow paths in butterfly valves, and (4) the most well-known losses attributed to rough surfaces or to flow paths including portions acting as bluff bodies.

In addition to the discharge loss coefficient found in Bernoulli's derived mass flow equations for single phase flow, the two-phase multiplier will now account for the above-mentioned losses.

These losses may vary significantly within any considered geometric configuration, thereby re-sults shows that a unique two-phase pressure drop multiplier relationship is valid only for a very specific designed section.

Figure 17 illustrates the behaviour of the two-phase frictional pressure drop multiplier for all seven geometric configurations and illustrates the behaviour of each two-phase pressure drop multiplier included in this study. Based on the similarity of the geometric configurations, results show close agreement between the two-phase pressure drop multipliers for the orifice plate and the gate valve. However, the behaviour of the two-phase pressure drop multiplier for the globe valve appears closer to the one established for the gate valve, but further apart from the one of the orifice plate. This variance reflects that globe valves have a different constriction than gate valves, thus have a more complex flow path, as the fluid undergoes a cyclic contraction and re-expansion. Furthermore, it appears clearly that the two-phase pressure drop multiplier for this work configuration shows high similarity with a Venturi-body one and is closer to the short-throat Venturi case.
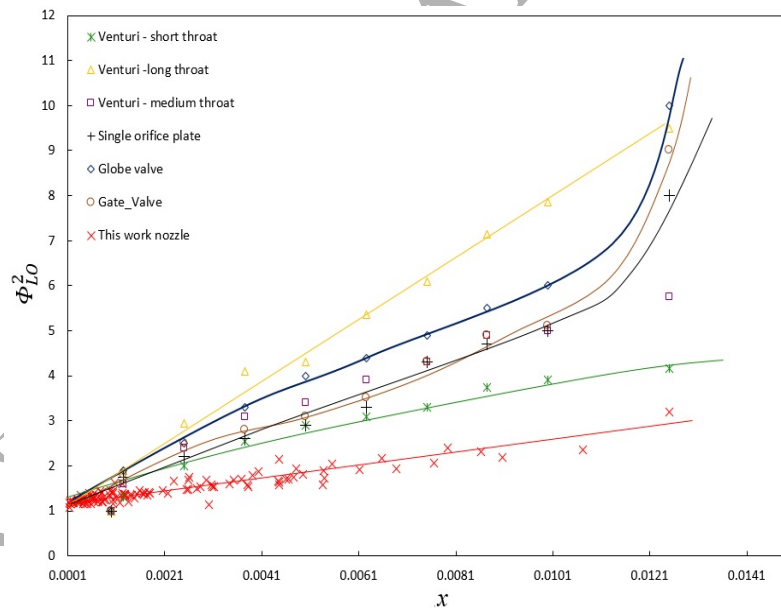

Figure 17: Comparison of this work two-phase multiplier against six other two-phase multipliers (having various geo-metrical configurations), up to flow quality x of 1.25%

It was also noted that there was a systematic variance in the two-phase pressure loss multi-plier resulting in a gradual and linear increase with the increase of the nozzle throat thickness.

For the studied geometric configuration which includes a convergent nozzle of negligible throat thickness, results showed a similar and lower two-phase multiplier than for the short-throat Venturi.

Based on the trend-lines established for this work and those of the Venturi-bodies, another expression was proposed and correlated for the two-phase pressure drop multiplier (for high liquid - low gas) $\Phi^2_{LO_{HL}}$, in terms of variance of the nozzle throat thickness and quality x. As illustrated in figure 18, the behaviour of the two-phase frictional pressure drop multiplier for all seven geometric configurations, a relationship of the variance of respective gradients m_Φ was determined in function of the throat thickness F (being a multiple of throat-diameter), which obeys a power law function of the form Ae^b, where values of A and b are given in figure 18, and the constant term c is equal to 1. Thereby, this can be expressed as:

$$\Phi^2_{LO_{HL}} = (AF^b * x) + c \tag{68}$$

which simplifies to:

$$\Phi^2_{LO_{HL}} = (382.62(F)^{0.418} * x) + 1 = \left[\frac{\dot{M}_{mix}}{C_{d_{liq}} * A_T}\right]^2$$
$$\left(\frac{\left(1-B^4\right)}{\left(2\rho_{liq}\Delta P_{mix}\right)}\right) = f(F, \ x) \tag{69}$$
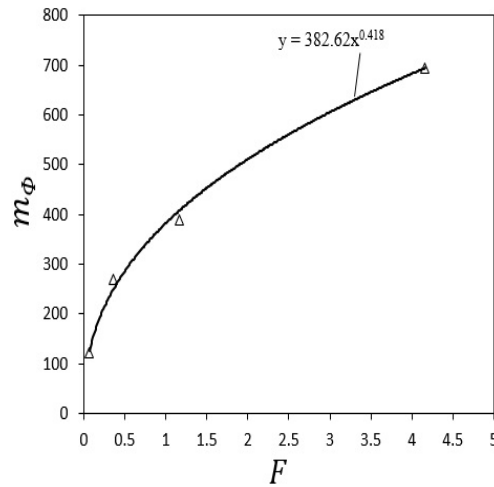
Figure 18: Two-phase multiplier gradient m_Φ v.s. throat thickness *[F]*.

5.3. Case B - high gas - low liquid

5.3.1. Case B (Method01) - high gas - low liquid

Results comprising (a) high gas - low liquid (*Method01*), and (b) high liquid - low gas data points are shown in figure 19. This figure clearly expresses the difference of behaviour between the two-cases. It mainly demonstrates a drastic increase of scattered data points for values $\alpha \geq$ 0.75. This effect signifies that the correlations satisfying a curvilinear behaviour within the high liquid - low gas region, are not valid to compute two-phase multipliers within the region of high gas - low liquid flows.

The scattering effect is more pronounced in figure 20(a) which displays the behaviour of all models considered. It appears even more clearly in figure 20(b) when comparing Morris's and this work correlations. Both plots show that it is very difficult to directly correlate the two-phase multiplier against the void fraction.

Such effect is primarily attributed to the Bernoulli equation. The two-phase multiplier (for high gas - low liquid), $\Phi^2_{LO_{HG}}$, was primarily calculated via the Bernoulli equation, including a fixed value equal to 1 for C_d, and a fixed liquid-water density. As this case involves high gas moving at high speeds through the nozzle throat, compressibility effects need to be accounted for. Such effects implicate variations of density (with the mixture density which can go down below 50 kg/m^3, hence a drastic change when compared to the 998 kg/m^3 density of liquid-water. This effect, if not accounted for, will eventually lead to too high estimated total mass flow-rates.
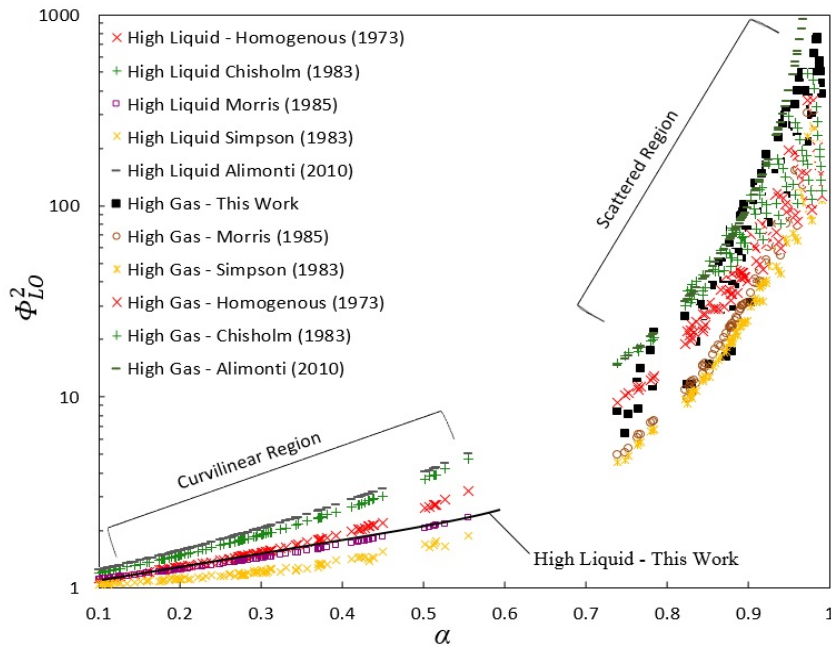
Figure 19: Void fraction α v.s. pressure-drop multiplier Φ^2_{LO}, for both reference models and this work.

This study identified two practical methods to account for such effect. The first method was based on a simple calculation involving an average operating density, i.e. an average value of the two-phase flow densities at upstream and downstream locations. This method is however an approximation only, and the average density value remains constant throughout the rest of the calculation. The second method exposed a novel approach using the Mach number Ma in the two-phase multiplier correlation. The Ma number was found for each data point via the ratio between the speed of the two-phase mixture at the throat (based on the momentum density which accounts for slippage, while adopting the Chisholm slip correlation) and the critical speed of sound for the same mixture conditions.

As noted in the methodology section, the introduction of the Mach number for two-phase flow conditions incurs a more complex calculation than for single-phase flows. An expression for c was derived from the well-known "frozen two-phase sonic velocity" model from Grolmes and Fauske (1970). The resulting Ma numbers caused the scattered data points (for $\Phi^2_{LO_{HG}}$ v.s. α) to segregate in lines of constant Ma numbers. This contributed in defining a set of curvilinear profiles while allowing an additional degree of freedom which could be either interpreted directly
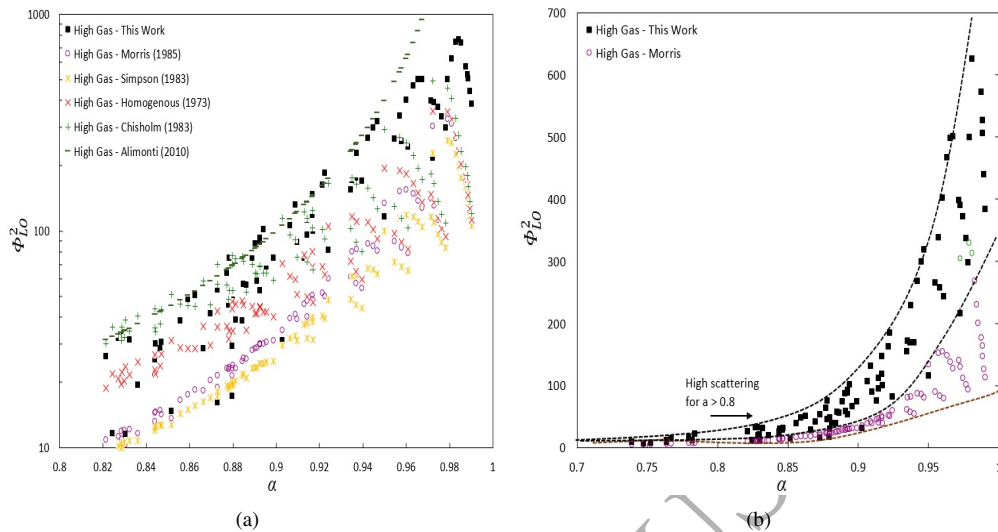
Figure 20: *(a)* Void fraction α v.s. pressure-drop Φ_{LO}^2 for both reference and this work correlations - illustrating drastic scattering within the high-end region for high gas - low liquid two-phase flow compositions; *(b)* Void fraction α v.s. pressure-drop multiplier Φ_{LO}^2 for Morris and this work correlations - illustrating drastic offset between the respective data trends.

from the plot, or based on a developed relationship, thus correlating directly the *Ma* number with both the void fraction α and the two-phase multiplier $\Phi_{LO_{HG}}^2$. The generated lines of constant *Ma* number are shown in figure 21.

Figure 22 shows another measure which considers the discrepancies between the actual and calculated total mass flow-rates. The relationship between the Mach number *Ma*, and a tuning parameter *I* shows a slight increase of *I*, thereby allowing an additional correction factor at higher mixture flow speeds.

Figure 23(a) and figure 23(b) illustrate the outcome when applying the developed correlation, for either estimating the frictional pressure drop using only the two-phase flow multiplier $\Phi_{lo_{HG}}^2$ as given in equation (60), or the total mass flow-rates when considering the combined relationship of *Cd_multi* and modified $\Phi_{lo_{HG}}^2$, via equation (53).
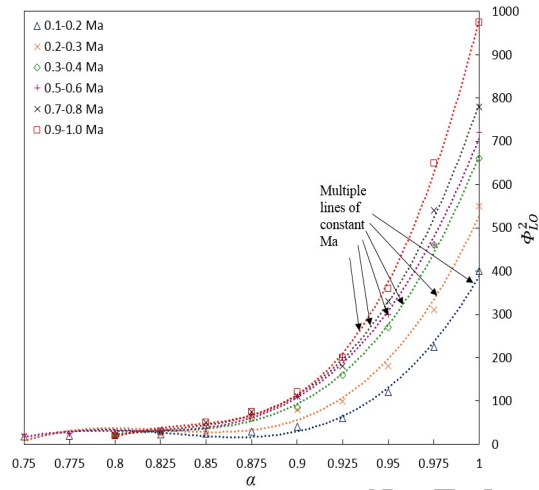
Figure 21: Void fraction α v.s. calculated pressure-drop multiplier Φ_{LO}^2 for this work correlation - segregated data via lines of constant Ma number.
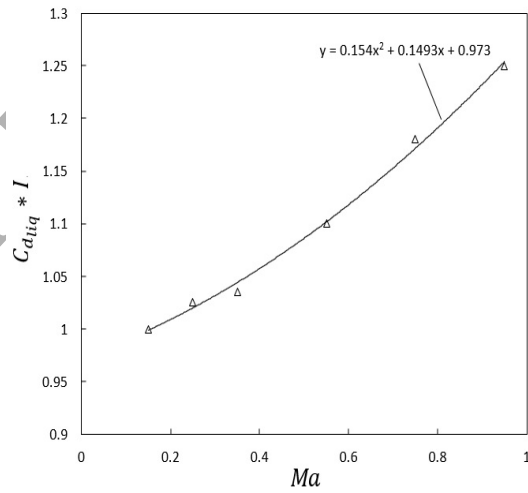

Figure 22: Mach number Ma against a tuning parameter $(C_{d_{liq}}) * I$.
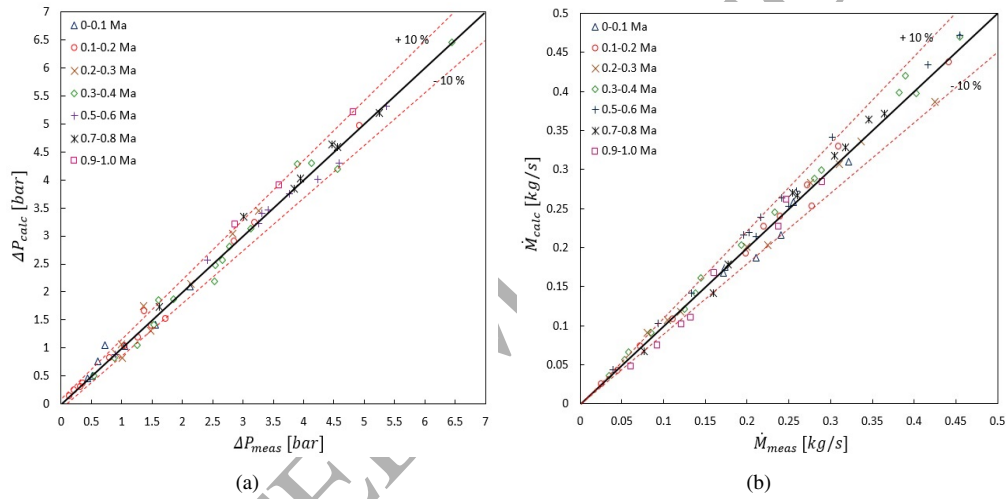
46

(a)   (b)

Figure 23: *(a)* Measured v.s. calculated frictional pressure drop using the final two-phase flow multiplier model - differentiating between data points according to respective *Ma* numbers; *(b)* Measured v.s. calculated total mass flow-rates *M* - differentiating between data points according to respective *Ma* numbers.

5.3.2. Case B (Method02) - high gas - low liquid

Results comprising high gas – low liquid data points, for (*Method02*) are shown in figure 24. The unmodified values of $\Phi^2_{lo_{HG}}$, obtained directly from equation (34), obey a trend-line expressed via a polynomial relationship of degree 2.
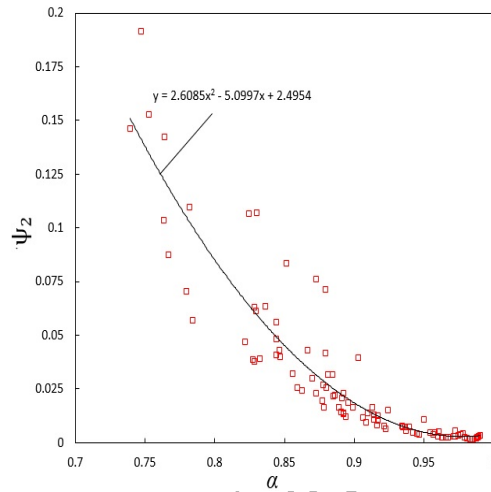

Figure 24: Void fraction α v.s. pressure-drop multiplier Φ^2_{LO} (not modified)

In addition, a second relationship, given by a calibration parameter Ψ_2, and in terms of α, allowed for the scattered data to fit within a curvilinear relationship. This multiple Ψ_2, followed a power law as illustrated in figure 25(a). The resultant of such calibration parameter led to the development of the proposed two-phase frictional pressure drop multiplier, as expressed by a polynomial relationship of degree 2, in figure 25(b).
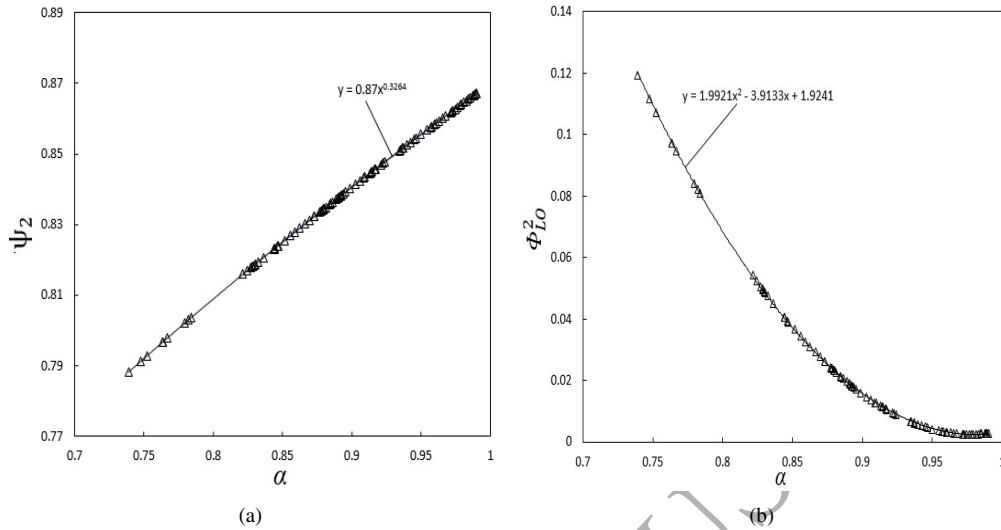
Figure 25: Tuning parameters. *(a)* Two-phase void fraction α v.s. tuning parameter Ψ_2 ; *(b)* Void fraction α v.s. modified pressure-drop multiplier Φ_{LO}^2.

Figure 26(a) illustrates the outcome of this study when applying the third developed correlation $\Phi_{lo_{HG}}^2$, given in equation (66), hence estimating the total mass flow-rates considering the variances due to ρ_{mix} and $C_{d_{multi}}$ directly in terms of $\Phi_{lo_{HG}}^2$, and substituted in equation (68).

Figure 26(b) shows a comparison between this work on two-phase pressure drop multiplier correlations for the high gas - low liquid, against the semi-empirical HEM-DS method. In this case, the results from the HEM-DS model are registered within a +/- 20 % error band. This confirms that the HEM-DS model (assuming no-flashing of liquid phase) is fairly applicable when considering that no frictional losses are accounted for. Note that in this comparison, it was found that the Simpson slip correlation gave better results, therefore using a power of y =1/6, with the two-phase discharge equation included for a discharge value of 0.975 for pure gas, and an average value of 0.90 for pure liquid. The other two-methods based on the two-phase multiplier methodologies were slightly more accurate than the aforementioned. It showed that the one involving the fundamental Mach number resulted in a +/- 10 % margin error.

This work has shown that despite the difficulties encountered to estimate frictional losses, a frictional factor should be included in the semi-empirical models discussed in this work.
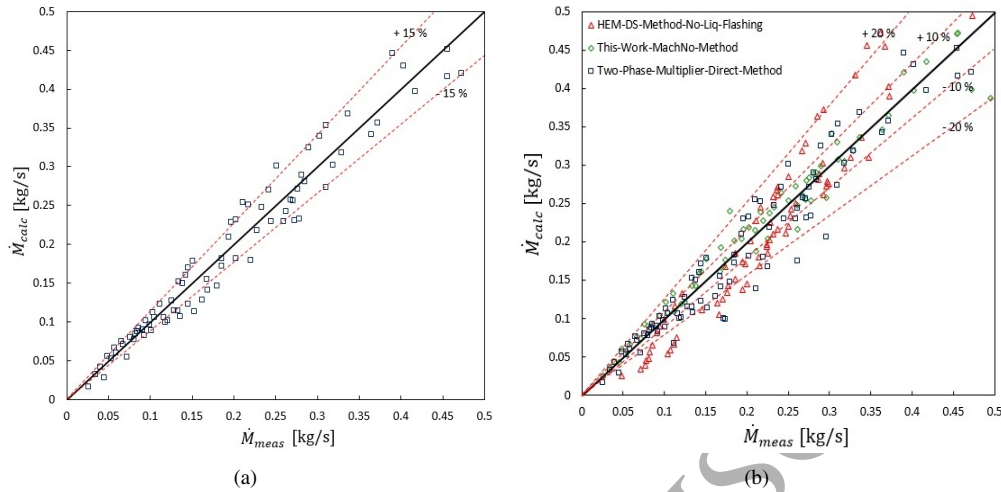
Figure 26: Measured v.s. calculated total mass flow-rates *M*. *(a)* this work second method for high gas - low liquid fluids; *(b)* comparison between this work Case B (1st and 2nd methods) and the HEM-DS method.

Figure 27 shows a comparison performed between this work experimental void fractions $\alpha_{experimental}$ and the predicted void fractions $\alpha_{predicted}$. The predicted void fractions were derived from the 20 referenced models, presented earlier in tables 1 and 2. To understand if there exists any similarity with any of the referenced model, a flow pattern independent analysis was used as the basis; this strategy was used to prevent any bias due to the flow pattern.

It appears that none of the correlations performed excellently-well, thus failed to correlate with less than 5 % error in both flow composition categories. To investigate this further, two pairs of plots were developed to show the average deviation and RMS errors between this work experimental void fraction and the referenced void fraction correlations.

The first pair of plots shown in figures 28(a) and 28(b) includes the first void-fraction category for values of $0 < \alpha \leq 0.55$. Figure 28(a) clearly demonstrates that four void fraction models, Chisholm (1983) slip-model, Chisholm (1983) homogeneous model, Armand (1946) slip-model and Huq and Loth (1992) slip-model (models 1, 18, 18 and 20 from tables 1 and 2 respectively) predicted this work experimental void fraction within a 10% error band. The good performance behaviour is also illustrated in figure 28(b), registering very low (< 0.015) RMSE values. The highest similarity was obtained with the Chisholm (1983) slip-model correlation.
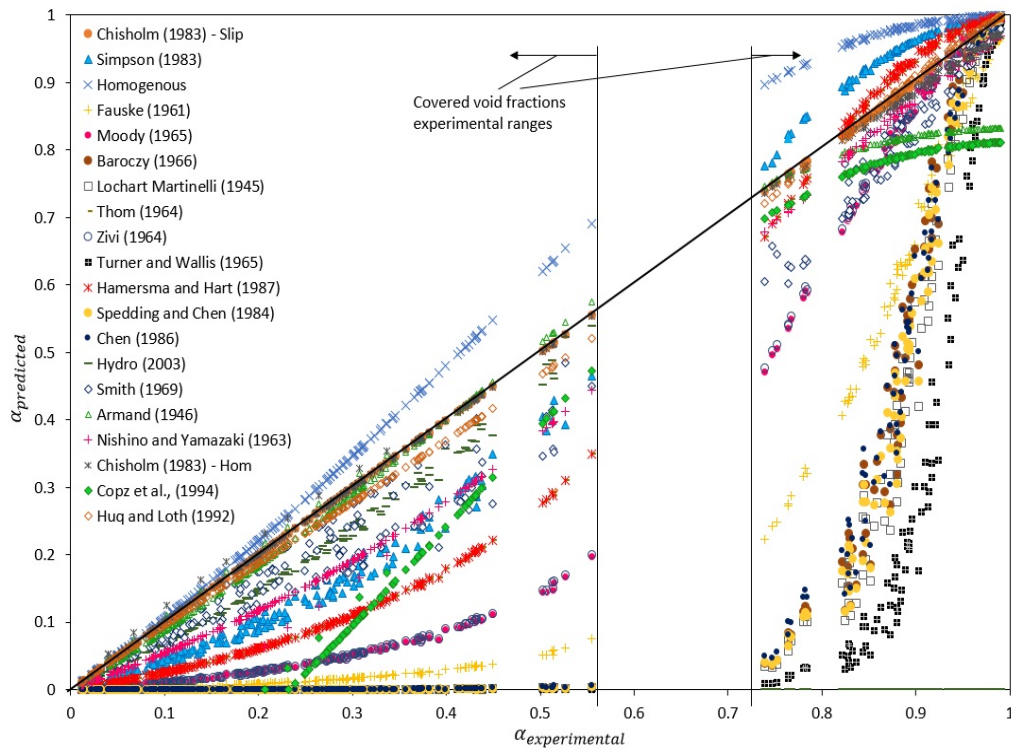
Figure 27: Comparative results of the measured void fractions to the predicted void fraction with the homogeneous, slip and other empirical models.
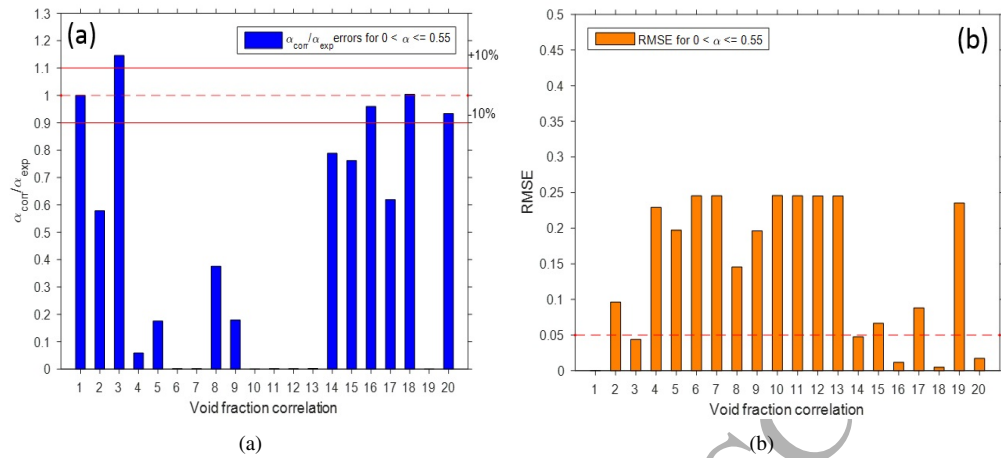
Figure 28: Void fraction correlations compared with the present work experimental void fractions for $0 < \alpha \leq 0.55$;*(a)* averaged standard deviation errors; *(b)* RMSE.

The second pair of plots shown in figures 29(a) and 29(b) includes the second void-fraction category for values $0.75 \leq \alpha < 1$. This time, 12 out of the 20 void fraction models tested were found within the ± 10 % error band: Chisholm (1983) slip-model, Simpson et al. (1983), Homogeneous, Moody (1965), Thom (1964), Zivi (1964), Schüller et al. (2003), Smith (1969), Armand (1946), Nishino and Yamazaki (1963), Chisholm (1983) Homogeneous, and Huq and Loth (1992) models, i.e. Models 1, 2, 3, 5, 8, 9, 14, 15, 16, 17, 18, and 20 in tables 1 and 2, respectively.

The RSME values shown in figure 29(b) agree with the error behaviour in figure 29(a). However, only void fraction models 8, 14, 17, 18 and 20 showed RMSE values less than 0.05 . The highest similarity was obtained by the Huq and Loth (1992) proposed correlation.

The effect of void fraction correlations on the two-phase pressure drop multiplier is presented in figure 30 and 31. This has been performed to compare the proposed correlations, expressed in terms of void fraction α, to the void fraction correlations described previously. Figure 30 shows the deviation of the two-phase pressure drop multiplier from equation (65) considering that the void fraction α is the experimental one from this work, or estimated from the best void fraction models shown in figure 29(a). It appears clearly that a highest deviation was obtained when considering the two-phase pressure drop multiplier. However, the void correlations of slip-models proposed by Chisholm (1983), Thom (1964), and Huq and Loth (1992) (Models 1, 8 and 20, respectively) proved satisfactory, with a deviation error less than 10 %.
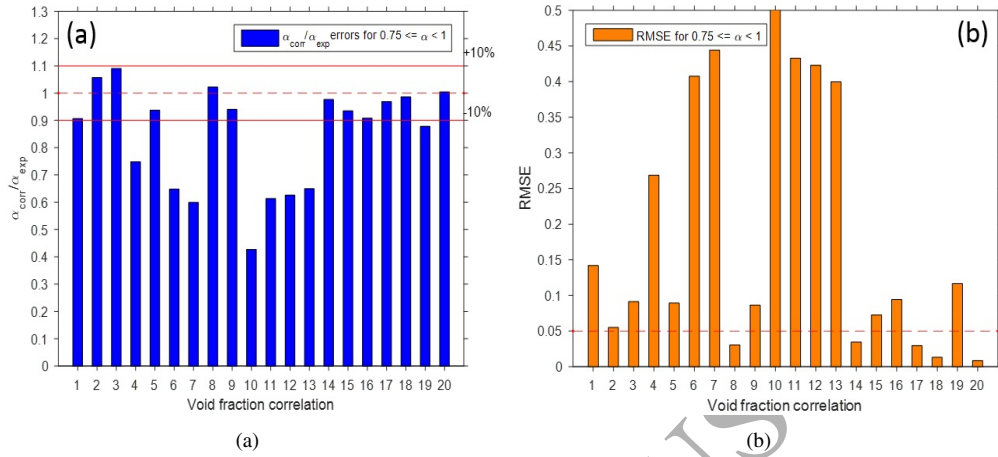
(a)

(b)

Figure 29: Void fraction correlations compared with the present work experimental void fractions for $0.75 \leq \alpha < 1$;*(a)* averaged standard deviation errors; *(b)* RMSE.
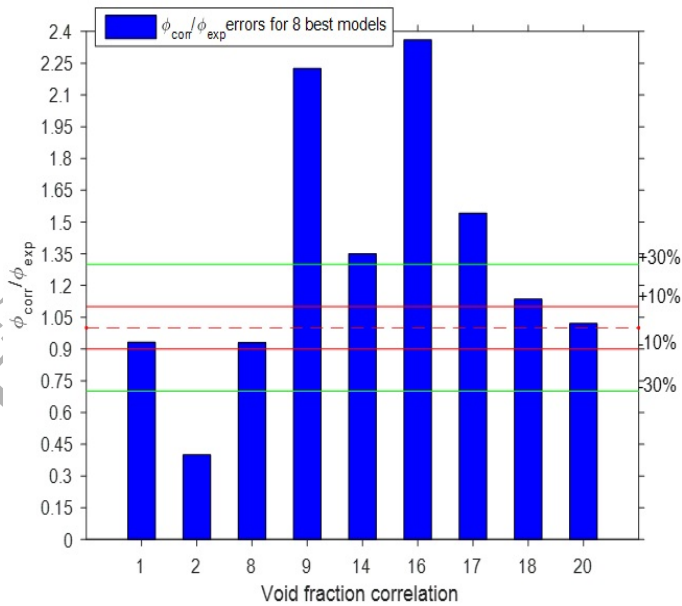

Figure 30: The average deviation from the two-phase pressure drop multiplier calculated from this work experimental void fraction for the proposed correlation presented in equation (65).

Figure 31 shows the deviation of the two-phase pressure drop multiplier from the developed correlation, equation (56). The deviation between this work and the selected 9 void fraction models were plotted for each of the 6 Mach number categories from table 4. Minimal variations in deviations are obtained for the variance in Mach number category, but a large deviation between the void correlation models is present. Four models performed fairly, the Chisholm (1983) - Slip model (Model 1), the Nishino and Yamazaki (1963) slip-model (Model 17) the Chisholm (1983) - Homogeneous model (Model 18) and the Huq and Loth (1992) - slip model (Model 20), with deviations inside a 30% bracket. It could therefore be concluded that there exists a similar behaviour between the two proposed correlations, although equation (65) performed slightly better than equation (56).
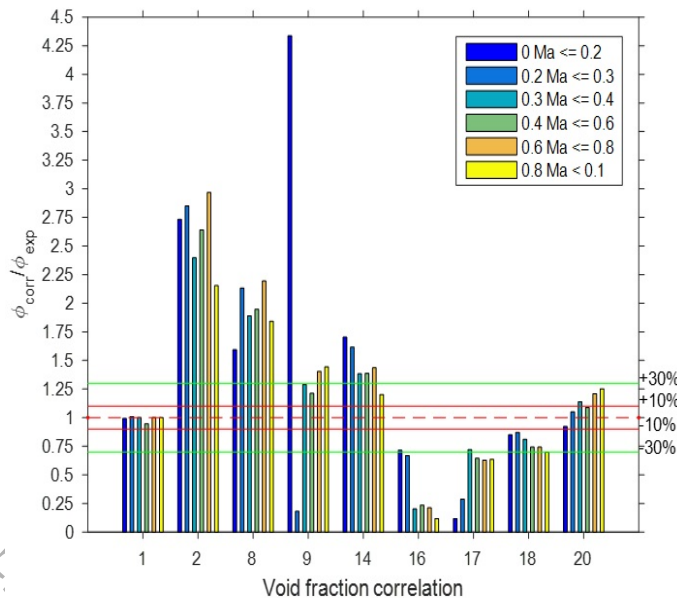

Figure 31: Average deviation from the two-phase pressure drop multiplier calculated with the present work experimental void fractions for the proposed correlation in equation (56).

Conclusions

In this study, the hydrodynamic characteristics of two-phase (air-water) mixtures through a conventional convergent nozzle were experimentally investigated. Based on the results generated, the following conclusions can be drawn:

1. The two-phase pressure drop multiplier for the case of high liquid - low gas flows can be approximated with the conventional correlation proposed by Morris (1985). A modification of the two-phase multiplier is needed to allow a variance of pressure drop, mainly due the variance of geometrical configuration.

2. Based on a unique experimental dataset, three empirical correlations were proposed for the two-phase pressure drop multiplier of a convergent nozzle.

   The first correlation covers two-phase (air-water) flows for $0 < \alpha \le 0.55$. The correlation includes a modification, in the form of a secondary multiplier, of the conventional correlation proposed by Morris (1985). The multiplier consists of a polynomial equation of degree 3 expressed in terms of void fraction α, which proved highly important to account for the effect due to discharge and geometric losses.

   For the same flow conditions comprising the high liquid - low gas region, a comparative study between various geometrical configuration devices (orifice, globe valve, gate valve and Venturi-tube) was performed. Results showed the significant effects of the geometry on the hydrodynamic characteristics of two-phase flows through different flow paths. Based on the similarity between this work in a nozzle and the Venturi-tube, a new correlation was proposed for the two-phase pressure drop in-terms of flow quality and throat thickness.

   The second correlation covers two-phase (air-water) flows with void fractions above 0.75. This method considered the variance of discharge coefficient under multiphase flow conditions separately from the frictional two-phase multiplier. In such case, it was shown that the two-phase multiplier obeys a polynomial form of degree 3, and is dependent on two main parameters: the void fraction, and the Mach number. The downside of applying such method is that it can only be used to calculate the total mass flow-rate (via lines of constant Mach number) provided that the two-phase flow velocity is a known value.

   Additionally, this work described a third two-phase pressure drop multiplier correlation. This correlation accounted for all variances mainly of density and discharge loss coefficient under two-phase (high gas - low liquid) flow conditions. The proposed two-phase frictional multiplier correlation can be directly applied to calculate the total mass flow with a maximum error band of +/- 15 %.

3. The developed empirical correlations were compared against the semi-empirical HEM-

DS model. This model failed to estimate mass flow-rates for two-phase flows with low quality, thus for mixtures within the high liquid - low gas region, but estimated the total mass flow-rates within a +/- 20 % margin error for two-phase fluids with a quality > 0.1, thus validating this work correlation for the high gas - low liquid.

4. In addition to the validation between predicted and measured total mass flow-rate values, the validation of the proposed two-phase pressure drop correlations were performed between the present work experimental void fraction values and the corresponding values derived from several void fraction correlations. Results showed that the Armand (1946) model, both Chisholm (1983) slip and homogeneous models, and the Huq and Loth (1992) void fraction model performed best, within an error band less than 5 % for $0 < \alpha \leq 0.55$. However, the Thom (1964), Schüller et al. (2003), Nishino and Yamazaki (1963), Chisholm (1983) and Huq and Loth (1992) void fraction models performed best, with an error band less than 5 % for $0.75 \leq \alpha < 1$. For both void fraction range-categories, the best models agreed with the performance described by their respective authors, as reported previously in tables 1 and 2.

The experimental results presented in this work enhanced the knowledge of the behaviour of two-phase flow through constrictions, such as in conventional design nozzle fixed within a vacuum chamber of an ejector device. The significance of such work validates the use of conical-nozzles configurations for simple and feasible monitoring flow metering devices. Based on a known pressure differential and void fractions (two simplistic measurable variables), the total mass flow-rates can be estimated through equations based on the proposed two-phase pressure drop multiplier correlations.

References

S. Morris, Two phase pressure drop across valves and orifice plates, Marchwood Engineering Laboratories, Southampton (1985).

D. Chisholm, Two phase flow in pipelines and heat exchangers, george godwin in association with the institution of chemical engineers, london (1983).

R. Huq, J. L. Loth, Analytical two-phase flow void prediction method, Journal of Thermophysics and Heat Transfer 6 (1992) 139–144.

C. Fairhurst, Component pressure loss during two-phase flow, in: International conference on the physical modelling of multi-phase flow, pp. 1–24, 1983.

C. Smoglie, J. Reimann, Two-phase flow through small branches in a horizontal pipe with stratified flow, International Journal of Multiphase Flow 12 (1986) 609–625.

F. S. Silva, P. Andreussi, P. Di Marco, Total mass flow rate measurement in multiphase flow by means of a venturi meter, Multiphase Production, Elsevier (1991) 145–155.

D. A. McNeil, Two-phase flow in orifice plates and valves, Proceedings of the Institution of Mechanical Engineers, Part C: Journal of Mechanical Engineering Science 214 (2000) 743–756.

A. Azzi, S. Belaadi, L. Friedel, Two-phase gas/liquid flow pressure loss in bends, Forschung im Ingenieurwesen 65 (2000) 309–318.

M. Fossa, G. Guglielmini, Pressure drop and void fraction profiles during horizontal flow through thin and thick orifices, Experimental Thermal and Fluid Science 26 (2002) 513–523.

C. Alimonti, G. Falcone, O. Bello, Two-phase flow characteristics in multiple orifice valves, Experimental Thermal and Fluid Science 34 (2010) 1324–1333.

A. Azzi, L. Friedel, Two-phase upward flow 90 bend pressure loss model, Forschung im Ingenieurwesen 69 (2005) 120–130.

X. Chen, B. S. McLaury, S. A. Shirazi, A Comprehensive Procedure to Estimate Erosion in Elbows for Gas/Liquid/Sand Multiphase Flow, Journal of Energy Resources Technology 128 (2006) 70.

S. Kim, G. Kojasoy, T. Guo, Two-phase minor loss in horizontal bubbly flow with elbows: 45 and 90 elbows, Nuclear Engineering and Design 240 (2010) 284–289.

L. Xing, H. Yeung, J. Shen, Y. Cao, Experimental study on severe slugging mitigation by applying wavy pipes, Chemical Engineering Research and Design 91 (2013) 18–28.

M. Gourma, P. Verdin, Two-phase slug flows in helical pipes: Slug frequency alterations and helicity fluctuations, International Journal of Multiphase Flow 86 (2016) 10–20.

A. Athulya, R. Miji Cherian, CFD Modelling of Multiphase Flow through T Junction, Procedia Technology 24 (2016) 325–331.

P. V. Mali, R. Singh, S. De, M. Bhatta, Downhole ESP & Surface Multiphase Pump - Cost Effective Lift Technology for Isolated and Marginal Offshore Field Development, in: SPE Asia Pacific Oil and Gas Conference and Exhibition, Society of Petroleum Engineers, 2013.

S. M. M. Sarshar, The Recent Applications of Jet Pump Technology to Enhance Production from Tight Oil and Gas Fields, in: SPE Middle East Unconventional Gas Conference and Exhibition, Society of Petroleum Engineers, 2012.

G. Falcone, G. Hewitt, C. Alimonti, B. Harrison, et al., Multiphase flow metering: current trends and future developments, in: SPE annual technical conference and exhibition, Society of Petroleum Engineers.

M. N. A. Beg, M. M. Sarshar, System for production boosting and measuring flow rate in a pipeline, 2015. US Patent App. 14/541,011.

W. Gilbert, Flowing and Gas-lift well Performance (1954).

R. F. Tangren, C. H. Dodge, H. S. Seifert, Compressibility Effects in Two-Phase Flow, Journal of Applied Physics 20 (1949) 637–645.

M. Grolmes, H. Fauske, Propagation characteristics of compression and rarefaction pressure pulses in one-component vapor-liquid mixtures, Nuclear Engineering and Design 11 (1970) 137–142.

R. E. Henry, H. K. Fauske, The Two-Phase Critical Flow of One-Component Mixtures in Nozzles, Orifices, and Short

Tubes, Journal of Heat Transfer 93 (1971) 179.

R. Sachdeva, Z. Schmidt, J. Brill, R. Blais, Two-Phase Flow Through Chokes, in: SPE Annual Technical Conference and Exhibition, Society of Petroleum Engineers, 1986.

Perkins, Critical and Subcritical Flow of Multiphase Mixtures Through Chokes - 20633, SPE Drilling and Completion 8 (1993) 271–276.

S. Selmer-Olsen, H. Lemonnier, Some mechanisms controlling high quality two-phase flows in convergent-divergent nozzles, Two-phase flow modelling and experimentation 1995 (1995) 933–941.

E. M. Alsafran, M. G. Kelkar, Predictions of Two-Phase Critical-Flow Boundary and Mass-Flow Rate Across Chokes, SPE Production & Operations 24 (2009) 249–256.

R. K. Haug, Multiphase Flow Through Chokes-Evaluation of five models for prediction of mass flow rates, Master's thesis, NTNU, 2012.

D. W. Green, R. H. Perry, Perry's Chemical Engineers' Handbook/edición Don W. Green y Robert H. Perry., C 660.28 P47 2008., 1973.

H. Simpson, D. Rooney, E. Grattan, Two phase flow through gate valves and orifice plates, in: International conference on the physical modelling of multi-phase flow, pp. 25–40, 1983.

Y. Taitel, A. Dukler, A theoretical approach to the lockhart-martinelli correlation for stratified flow, International Journal of Multiphase Flow 2 (1976) 591–595.

D. Chisholm, Two-phase flow in pipelines and heat exchangers, G. Godwin in association with Institution of Chemical Engineers, 1983.

T. Lenzing, L. Friedel, J. Cremers, M. Alhusein, Prediction of the maximum full lift safety valve two-phase flow capacity, Journal of Loss Prevention in the Process Industries 11 (1998) 307–321.

J. C. Leung, A theory on the discharge coefficient for safety relief valve, Journal of Loss Prevention in the Process Industries 17 (2004) 301–313.

R. Darby, On two-phase frozen and flashing flows in safety relief values: Recommended calculation method and the proper use of the discharge coefficient, Journal of Loss Prevention in the Process Industries 17 (2004) 255–259.

R. Darby, K. Molavi, Viscosity correction factor for safety relief valves, Process Safety Progress 16 (1997) 80–82.

R. Diener, J. Schmidt, Sizing of throttling device for gas/liquid two-phase flow part 1: Safety valves, Process Safety Progress 23 (2004) 335–344.

R. E. Henry, H. K. Fauske, S. T. McComas, Two-Phase Critical Flow at Low Qualities Part I: Experimental, Nuclear Science and Engineering 41 (1970) 79–91.

M. A. Woldesemayat, A. J. Ghajar, Comparison of void fraction correlations for different flow patterns in horizontal and upward inclined pipes, International Journal of Multiphase Flow 33 (2007) 347–370.

R. t. Martinelli, Prediction of pressure drop during forced circulation boiling of water, Trans. Asme 70 (1948) 695–701.

S. L. Smith, Void Fractions in Two-Phase Flow: A Correlation Based upon an Equal Velocity Head Model, Proceedings of the Institution of Mechanical Engineers 184 (1969) 647–664.

C. Baroczy, Correlation of liquid fraction in two-phase flow with application to liquid metals (1963).

D. Butterworth, A COMPARISON OF SOME VOID-FRACTION RELATIONSHIPS FOR CO-CURRENT GAS-LIQUID FLOW, Int. J. Multiphase Flow 1 (1975) 845–850.

M. A. Grolmes, J. C. Leung, Code method for evaluating integrated relief phenomena, Chemical engineering progress

81 (1985) 47–52.

N. Mathure, Study of flow patterns and void fraction in horizontal two-phase flow, Oklahoma State University, 2010.

I. Fauske, Crilical-two-phase, steam-water flows, heat transfer and fluid mechanics institute, 1961.

F. J. Moody, Maximum Flow Rate of a Single Component, Two-Phase Mixture, Journal of Heat Transfer 87 (1965) 134.

C. Baroczy, A systematic correlation for two-phase pressure drop, Technical Report, Atomics International, Canoga Park, Calif., 1966.

R. Lockart, R. Martinelli, Proposed correlation of data for isothermal two-phase, two-component flow in pipes, Chem. Eng. Prog 45 (1949) 39–48.

J. R. S. Thom, PREDICTION OF PRESSURE DROP DURING FORCED CIRCULATION BOILING OF WATER, IIll. .I. Hlwf iuas Twuftv 7 (1964) 7–724.

S. M. Zivi, Estimation of Steady-State Steam Void-Fraction by Means of the Principle of Minimum Entropy Production, Journal of Heat Transfer 86 (1964) 247.

J. Turner, G. Wallis, The separate-cylinders model of two-phase flow, paper no, NYO-3114-6Thayer's School Eng., Dartmouth College, Hanover, NH, USA (1965).

P. Hamersma, J. Hart, A pressure drop correlation for gas/liquid pipe flow with a small liquid holdup, Chemical Engineering Science 42 (1987) 1187–1196.

P. Spedding, J. Chen, Holdup in two phase flow, International Journal of Multiphase Flow 10 (1984) 307–339.

J. Chen, A further examination of void fraction in annular two-phase flow, International Journal of Heat and Mass Transfer 29 (1986) 1760–1763.

R. Schüller, T. Solbakken, S. Selmer-Olsen, Evaluation of Multiphase Flow Rate Models for Chokes Under Subcritical Oil/Gas/Water Flow Conditions, SPE Production & Facilities 18 (2003) 170–181.

Armand, The resistance during the movement of a two-phase system in horizontal pipes, Izvestiia Vsesoiuznyi Teplotekhnicheskii Institut 1 (1946) 16–23.

H. Nishino, Y. Yamazaki, A new method of evaluating steam volume fractions in boiling systems, Nippon Genshiryoku Gakkai-Shi 5 (1963).

V. Czop, D. Barbier, S. Dong, Pressure drop, void fraction and shear stress measurements in an adiabatic two-phase flow in a coiled tube, Nuclear Engineering and Design 149 (1994) 323–333.

G. Gregory, L. Mattar, An In-Situ Volume Fraction Sensor For Two-Phase Flows of Non-Electrolytes, Journal of Canadian Petroleum Technology 12 (1973).

R. Rosehart, E. Rhodes, D. Scott, Studies of gas-liquid (non-newtonian) slug flow: void fraction meter, void fraction and slug characteristics, The Chemical Engineering Journal 10 (1975) 57–64.

N. Tsochatzidis, T. Karapantsios, M. Kostoglou, A. Karabelas, A conductance probe for measuring liquid fraction in pipes and packed beds, International Journal of Multiphase Flow 18 (1992) 653–667.

K. J. Elkow, K. S. Rezkallah, Void fraction measurements in gas - liquid flows using capacitance sensors, Measurement Science and Technology 7 (1996) 1153–1163.

C.-H. Song, M. K. Chung, H. C. No, Measurements of void fraction by an improved multi-channel conductance void meter, Nuclear Engineering and Design 184 (1998) 269–285.

M. Fossa, G. Guglielmini, A. Marchitto, Intermittent flow parameters from void fraction analysis, Flow Measurement and Instrumentation 14 (2003) 161–168.

M. S. Ko, B. A. Lee, W. Y. Won, Y. G. Lee, D. W. Jerng, S. Kim, An improved electrical-conductance sensor for void-fraction measurement in a horizontal pipe, Nuclear Engineering and Technology 47 (2015) 804–813.

J. M. Mandhane, G. A. Gregory, K. Aziz, A flow pattern map for gas-liquid flow in horizontal pipes, Int. J. Multiphase Flow 1 (1974) 537–553.

H. Simpson, D. Rooney, E. Grattan, Two phase flow through gate valves and orifice plates, in: International conference on the physical modelling of multi-phase flow, pp. 25–40.